AGU PUBLICATIONS

JGR

Journal of Geophysical Research: Oceans

RESEARCH ARTICLE

10.1002/2017JC013231

Bottom Water Acidification and Warming on the Western Eurasian Arctic Shelves: Dynamical Downscaling Projections

P. J. Wallhead[1], R. G. J. Bellerby[1,2], A. Silyakova[3], D. Slagstad[4], and A. A. Polukhin[5]

[1]Norwegian Institute for Water Research, Bergen, Norway, [2]SKLEC-NIVA Centre for Marine and Coastal Research, State Key Laboratory for Estuarine and Coastal Research, East China Normal University, Shanghai, China, [3]Department of Geosciences, Centre for Arctic Gas Hydrate, Environment and Climate, Arctic University of Norway, Tromsø, Norway, [4]SINTEF Ocean AS, Trondheim, Norway, [5]Shirshov Institute of Oceanology, Russian Academy of Sciences, Moscow, Russia

Abstract The impacts of oceanic CO_2 uptake and global warming on the surface ocean environment have received substantial attention, but few studies have focused on shelf bottom water, despite its importance as habitat for benthic organisms and demersal fisheries such as cod. We used a downscaling ocean biogeochemical model to project bottom water acidification and warming on the western Eurasian Arctic shelves. A model hindcast produced 14–18 year acidification trends that were largely consistent with observational estimates at stations in the Iceland and Irminger Seas. Projections under SRES A1B scenario revealed a rapid and spatially variable decline in bottom pH by 0.10–0.20 units over 50 years (2.5%–97.5% quantiles) at depths 50–500 m on the Norwegian, Barents, Kara, and East Greenland shelves. Bottom water undersaturation with respect to aragonite occurred over the entire Kara shelf by 2040 and over most of the Barents and East Greenland shelves by 2070. Shelf acidification was predominantly driven by the accumulation of anthropogenic CO_2, and was concurrent with warming of 0.1–2.7°C over 50 years. These combined perturbations will act as significant multistressors on the Barents and Kara shelves. Future studies should aim to improve the resolution of shelf bottom processes in models, and should consider the Kara Sea and Russian shelves as possible bellwethers of shelf acidification.

Key Points:
- Downscaling ocean model reproduces observed 14–18 year acidification trends (0.015–0.025 per decade) at high northern latitudes
- Shelf bottom acidification and warming under SRES A1B is rapid and spatially variable (0.10–0.20 pH and 0.1–2.7°C over 50 years)
- Acidification and warming may stress benthic and demersal organisms on the Norwegian, Barents, Kara, and East Greenland shelves

Supporting Information:
- Supporting Information S1

Correspondence to:
P. Wallhead,
philip.wallhead@niva.no

Citation:
Wallhead, P. J., Bellerby, R. G. J., Silyakova, A., Slagstad, D., & Polukhin, A. A. (2017). Bottom water acidification and warming on the western Eurasian Arctic shelves: Dynamical downscaling projections. *Journal of Geophysical Research: Oceans*, *122*, 8126–8144. https://doi.org/10.1002/2017JC013231

Received 30 JUN 2017
Accepted 24 SEP 2017
Accepted article online 27 SEP 2017
Published online 25 OCT 2017

1. Introduction

The oceans have helped to mitigate global warming by absorbing a large portion of the anthropogenic CO_2 emissions (25%–29% during 2006–2015, Le Quéré et al., 2016), but as a result the CO_2 chemistry of seawater has been impacted, a process known as ocean acidification (OA) (Caldeira & Wickett, 2003; Ciais et al., 2013; Doney et al., 2009; Orr et al., 2005). Absorbed CO_2 reacts with seawater with the net effect of increasing the hydrogen ion concentration (decreasing the pH) and decreasing the carbonate ion concentration, thus decreasing the saturation state with respect to calcium carbonate. These changes may stress marine organisms by disrupting a wide range of physiological processes (Pörtner, 2008; Pörtner et al., 2014) including the construction and maintenance of shells (Fabry et al., 2008). High northern latitudes are particularly susceptible to OA because here the climatic pH decreases are amplified (Bellerby et al., 2005; Bopp et al., 2013; Ciais et al., 2013; Frolicher & Joos, 2010; Steinacher et al., 2009) and saturation states were already low in preindustrial times (Feely et al., 2009; Steinacher et al., 2009), so critical thresholds are likely to be reached earlier (Ciais et al., 2013; Fabry et al., 2009; Steinacher et al., 2009).

The oceans have also absorbed most of the heat energy that has been trapped by global warming (93% during 1971–2010, Rhein et al., 2013), causing warming of ~0.1°C per decade globally in the upper 70 m (Rhein et al., 2013). The Barents Sea in the Arctic Ocean has been identified as a hot spot of ocean warming over the last three decades (~1°C per decade, Levitus et al., 2009) and over this century (Biastoch et al., 2011; Bopp et al., 2013; Renaud et al., 2015). Ocean warming can cause changes in species abundance and distribution and significant ecosystem shifts, with potentially large socioeconomic implications, even for regional multidecadal warming of ~1°C associated with natural climate variations (IPCC "high confidence") (Pörtner et al., 2014). Vulnerability may be greatest in polar animals due to their narrow temperature ranges and lack of options for migrating to higher latitudes ("medium confidence"). At high northern latitudes, the combined stresses of warming, acidification, and deoxygenation acting in synergy (Denman et al., 2011; Kroeker et al., 2013; Pörtner, 2008) are expected to be important this century (Bopp et al., 2013; Henson et al., 2017).

In this study, we use an ocean biogeochemical model to project acidification and warming on the western Eurasian Arctic shelves, focusing on changes over the next 50 years. A novel aspect is that we also focus on shelf bottom water at depths 50–500 m. This defines the habitat for a host of benthic (seafloor-dwelling) organisms including calcifiers such as mollusks and corals, which are highly sensitive to OA as groups (Kroeker et al., 2013; Wittmann & Pörtner, 2013), and which play important roles in biogeochemical cycles and the marine food web. It also includes habitats for demersal fish such as cod and their more sensitive larval stages (Frommel et al., 2012; Stiasny et al., 2016). We hypothesize that these waters may see some of the strongest impacts of climatic change in the coming decades, because they are shallow enough that significant changes can occur on multidecadal time scales, but generally deep enough to avoid the strong seasonal and subseasonal variability that may make surface-dwelling organisms more tolerant of baseline changes (Hauri et al., 2013; Henson et al., 2017).

A second novel aspect of our study is the use of a dynamical downscaling ocean model, whereby output from global climate models is used to drive a regional model with higher spatial resolution. The need for higher spatial resolution, relative to present climate models, has been highlighted by Popova et al. (2014) and Steiner et al. (2014) for the Arctic Ocean and by Holt et al. (2014, 2017) for shelf seas in general. The extra resolution obtained by dynamical downscaling has been found to significantly improve transports of heat and salt by Atlantic currents flowing into the North Sea (Ådlandsvik, 2008; Ådlandsvik & Bentsen, 2007) and the Barents Sea (Melsom et al., 2009; Sandø et al., 2014).

A notable caveat of this study is that we do not consider possible gradients across the lower benthic/diffusive boundary layer where current speed and turbulence are strongly inhibited by bottom friction (Dade et al., 2001). Gradients can develop here due to reduced vertical mixing, the very different CO_2 chemistry of the sediments, and possible biological perturbations (Anthony et al., 2011; Cornwall et al., 2014). For this reason, we use the term "bottom water" rather than "seafloor." Also, we do not consider possible additional carbon inputs from thawing permafrost (subsea or land derived) which could significantly exacerbate bottom acidification (Biastoch et al., 2011; Semiletov et al., 2016). Finally, as our work is motivated by providing environmental projections for an impact study on Arctic benthic calcifiers, we focus less on understanding model fluxes and mechanisms and more on the accuracy of the historical state and bias correcting the future projections, although we do discuss the impact of model uncertainties and how they might be addressed in future work.

2. Materials and Methods

2.1. SINMOD (SINtef MODel)

SINMOD (http://sinmod.no/) is a 3-D ocean biogeochemical model coupling a hydrodynamic model based on the primitive Navier-Stokes equations (Slagstad & McClimans, 2005), an ice model similar to that of Hibler (1979), and a planktonic food web model (Wassmann et al., 2006). The pan-Arctic configuration used here has ocean boundaries in the North Atlantic and Bering Strait (see Figure 1), a Cartesian horizontal grid with resolution of 20 km, and 25 vertical layers with fixed depth ranges (z-levels) spanning: 0–10, 10–15, 15–20, 20–25, 25–30, 30–35, 35–40, 40–50, 50–75, 75–100, 100–150, 150–200, 200–250, 250–300, 300–400, 400–500, 500–700, 700–1,000, 1,000–1,500, 1,500–2,000, 2,000–2,500, 2,500–3,000, 3,000–3,500, 3,500–4,000, and 3,500–4,500 m. For more details on the hydrodynamic and sea-ice components see Slagstad and McClimans (2005) and Slagstad et al. (2015).

Biogeochemical state variables include ammonium, nitrate, and silicate as inorganic nutrients, two phytoplankton groups (diatoms and autoflagellates), fast and slow sinking detritus, labile dissolved organic carbon (DOC), refractory colored dissolved organic matter (cDOM, units μmolC/L), bacteria, heterotrophic nanoflagellates, microzooplankton, and two groups of mesozooplankton: the Atlantic *Calanus finmarchicus* and the Arctic *Calanus glacialis* (see Wassmann et al., 2006, for more details). Organic matter entering the bottom sediments is remineralized at a constant rate of 5% per day. In order to match annual estimates of denitrification on the Arctic continental shelves, 40% of the remineralized nitrogen is released as N_2 (Chang & Devol, 2009; Kaltin & Anderson, 2005). cDOM is input by rivers, decays at a constant rate of 0.55% per day, and contributes $0.023 \times \text{cDOM}\ m^{-1}$ to the diffuse attenuation of photosynthetic available radiation.

The CO_2 system module in SINMOD (Bellerby et al., 2012) is built in the hydrodynamic model and interacts with the food web model through the biological uptake of inorganic carbon by primary producers and

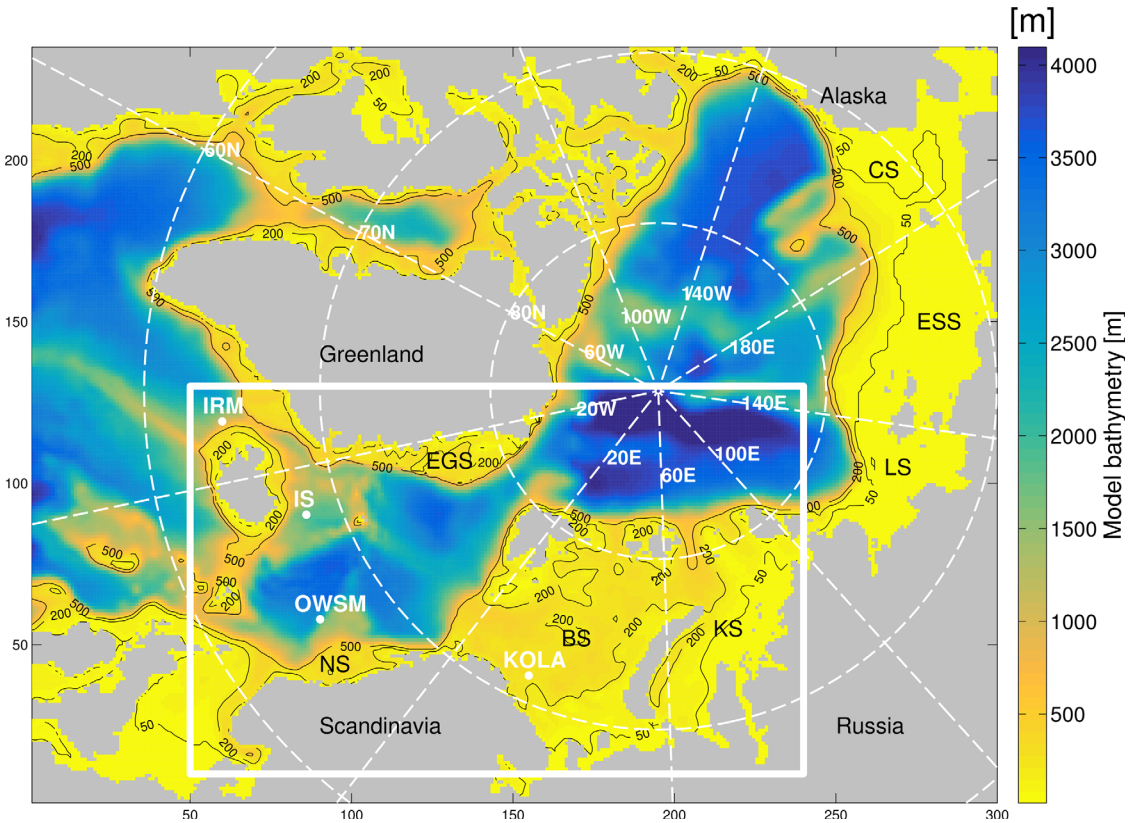

Figure 1. SINMOD bathymetry (water depth) for the full model domain. Black lines show 50, 200, and 500 m contours. The white square shows the study region, and the white spots show the positions of time series stations used for model validation: IRM, Irminger Sea; IS, Icelandic Sea; OWSM, Ocean Weather Station M; KOLA, Russian Kola section (average position). NS, Norwegian Shelf; BS, Barents Sea; KS, Kara Sea; EGS, East Greenland Shelf; LS, Laptev Sea; ESS, East Siberian Shelf; CS, Chukchi Sea.

inorganic carbon release due to organic matter respiration. Dissolved inorganic carbon (DIC) and total alkalinity (Alk) are fully prognostic state variables that are input by rivers, exchanged with the atmosphere (DIC only), and produced/consumed by plankton and bacteria following the nutrient-H^+ compensation principle (Wolf-Gladrow et al., 2007). Along with nutrients and salinity (S), DIC and Alk can be stored in ice during freezing, transported horizontally within the ice, and released during ice melt in summer. During ice formation, 30% of (nutrients, S, DIC, Alk) are released into the water column. As the ice ages there is a loss of brine (nutrients, S, DIC, Alk) to the water column at a rate dependent on ice temperature.

SINMOD total hydrogen ion-scale pH and saturation states were calculated diagnostically from output for (DIC, Alk, temperature [T], S, silicate) using CO2SYS.m (van Heuven et al., 2011) with optional dissociation constants from Millero (2010), Dickson (1990), and Uppström (1974). For these calculations, we used regression functions fitted to CARINA data to estimate water pressure from depth and phosphate concentration from modeled (T, silicate, nitrate).

2.2. Hindcast Run (1975–2008)

For the hindcast run, atmospheric forcing was provided by reanalysis data from the European Centre for Medium-Range Weather Forecasts (ECMWF) ERA40 data set before 2003 and by ERA INTERIM beyond 2002 (Dee et al., 2011). Atmospheric CO_2 concentrations were derived from observations at Ocean Weather Station Mike (OWSM, 66°N, 2°E). Freshwater fluxes (river discharges and diffuse run-off from land) were based on hydrological model simulations for the Norwegian coast and Barents Sea (Dankers & Middelkoop, 2007) and for the Arctic rivers on observations from R-ArcticNet (Vörösmarty et al., 1996, 1998). Riverine concentrations of (DIC, Alk, nutrients, and DOC) were specified as constant values based on observations where available (Amon & Meon, 2004; Cooper et al., 2008; Dittmar & Kattner, 2003), otherwise default values were applied (supporting information Table S1). Riverine (DIC, Alk) were assumed equal (Fransson et al., 2001)

except for the Baltic "river" where values (1,540, 1,560) μmol/kg were used. A total of eight tidal components were imposed (elevation and currents) at the open boundaries using data from the TPXO 6.2 model of global ocean tides (www.coas.oregonstate.edu/research/po/research/tide/global.html).

Boundary fluxes of seawater were kept constant during the simulation: a total of 0.8 Sv enters the model domain through the Bering Strait (Woodgate et al., 2010) while on the Atlantic side the average fluxes were taken from a large-scale (50 km resolution) model covering most of the North Atlantic. Boundary conditions for (T, S, nitrate, silicate, DIC, and Alk) were derived (Bellerby et al., 2012) from the Bergen Earth system model (BCM-C, Tjiputra et al., 2010), bias corrected toward the CARbon IN the Atlantic (CARINA) data set (Key et al., 2010) using an absolute delta change method (Hay et al., 2000). CARINA data were first projected onto the boundary horizontal-depth grid and compared with BCM output at the same time and projected location; bias for each boundary grid cell was then calculated as an average of BCM-CARINA differences weighted by projection distance, and finally the biases were smoothed over the boundary grid. Since most of the CARINA observations are from the spring-summer season, a separate bias was calculated for winter values using the CARINA data interpolated to wintertime mixed layer depths (as reported by Steinhoff et al., 2010) as estimates of winter mixed layer values.

SINMOD was initialized with (T, S) fields from the World Ocean Circulation Experiment (WOCE) data set Version 3.0 (Lindstrom, 2001) and (nutrients, DIC, Alk) fields derived from the CARINA data set. The model was run for 20 repeated years spin-up using forcings and boundary conditions for 1975 to provide an initial condition, then for the 24 years 1975–2008 to generate the hindcast output. SINMOD bottom water values were taken as the deepest grid cell not in the land mask at each horizontal location.

2.3. Observational Data

Data were collated from: the World Ocean Database (WOD Ocean Station Data, Boyer et al., 2013), the International Council for the Exploration of the Sea Dataset on Ocean Hydrography (ICES, Copenhagen, 2013), the Global Ocean Data Analysis Project, version 2 (GLODAPv2, Key et al., 2015; Olsen et al., 2016), the CARINA Iceland and Irminger Sea Time Series version 2 (Olafsson et al., 2009a, 2009b), and a set of cruise data from the Kara Sea provided by the Shirshov Institute on Oceanology (hereafter the "Russian data"). For the WOD data, we used only data with observed level quality-control (QC) flag = 0 ("accepted value"). For GLODAPv2 and CARINA data, we required primary QC flag = 0 ("approximated"), 2 ("good"), or 6 ("replicated"; Key et al., 2010; Olsen et al., 2016), and for the Russian data, we excluded any values flagged as extrapolated to depth. We used data from (WOD, ICES, GLODAPv2, Russian) data sets for (T, S, nutrients) and from (GLODAPv2, CARINA, Russian) data sets for CO_2 chemistry variables.

In order to maximize the CO_2 chemistry data coverage, the GLODAPv2 and CARINA data sets were merged and parsed, and equilibrium values were recalculated using CO2SYS.m with constants as for the SINMOD calculations and missing silicate/phosphate data filled by kernel smoothing in 3-D (x,y,z) (Hastie et al., 2009). We refer to this extended data set as GLODAPv2E. The Russian CO_2 chemistry data originally included (Alk, pH) pairs with pH reported on the NBS scale. Again, CO2SYS.m with the aforementioned constants was used to convert pH to total scale and to calculate the corresponding (DIC, Ω). These Russian data are treated with additional caution because the measurement methods, although careful (see supporting information Text S1), do not conform to standard international protocols (Dickson et al., 2007) and because of inherent uncertainties associated with the use of the NBS scale (Dickson, 1984, see also Olsen et al., 2016).

To estimate bottom water values, we extrapolated profiles to estimated seafloor depths by kernel smoothing with an exponential kernel, extrapolating by up to 30% of the sampled depth range (otherwise discarding the profile), and varying the smoothing bandwidth and order (linear or constant) according to data coverage to ensure robust extrapolations. Water depth was estimated by interpolating high-resolution bathymetry products (the 500 m resolution IBCAOv3, Jakobsson et al., 2012, where available, otherwise the 2 min ETOPOv2, National Geophysical Data Center, 2006) and corrected to the maximum sampled depth wherever this exceeded the interpolated depth.

2.4. Model Skill Assessment and Bias Estimation

To assess model skill, SINMOD bottom water output was linearly interpolated in 3-D (x,y,t) to the observational data, and "errors" were computed as the model-minus-data differences. This was done for all data during years 1984–2008 inclusive (the first five hindcast years are avoided to minimize spin-up effects).

Point-to-point skill metrics were then computed as the root-mean-square error (RMSE), bias (mean error), and Pearson linear correlation (denoted by CORR or r), considering all model-data pairs at depths 50–500 m within the study region (white square in Figure 1).

For (T, S) regional bias fields were estimated by kernel-smoothing the errors in 2-D (x,y) using a Gaussian kernel with bandwidth 40 km. For CO_2 chemistry and nutrient variables, observational data coverage was considered insufficient for spatial smoothing (see supporting information Figures S1 and S2); instead, errors were aggregated as a function of model water depth over the entire pan-Arctic domain, and natural cubic spline functions with knots at 20, 50, 100, 200, 300, 400, 500, 1,000, and 2,000 m were fitted by ordinary least squares linear regression (Hastie et al., 2009). Only the GLODAPv2E data were used for bias-correction and skill assessment of CO_2 chemistry variables. Note that by using model-data errors from coincident times (and positions), we mitigate the effects of temporal sampling bias, but if there is strong seasonal or interannual variability in the errors then estimates may yet be biased toward better-sampled seasons or years (supporting information Table S2). However, we did not find large differences between overall bias estimates formed by averaging estimates over seasonal or yearly bins versus without binning (supporting information Tables S3 and S4), suggesting that the effects of temporal sampling bias were not strong at least on the regional scale.

The most relevant aspect of model skill for this study is the ability to simulate long-term or climatic temporal trends. There are only a few places where such trends have been measured for seawater variables at high northern latitudes, but four of these fall (by design) within our study region: the Irminger Sea time series (IRM), the Icelandic Sea time series (IS), the Ocean Weather Station M time series (OWSM), and the Kola Section time series (see Figure 1). For these stations, we derived temporal trend estimates with confidence intervals for time series data from observations and from SINMOD output interpolated to the station locations and sampling depths. This was done by fitting seasonal first-order autoregressive (AR1) models to data preaveraged by season and restricted to a common interval (the sampled interval within the hindcast test period 1984–2008). Significance of trend differences was tested by fitting the same time series model to the model-data errors (interpolating SINMOD over space and time to the observations) and applying a *t* test to the fitted trend parameter, accounting for AR1 serial correlation (Wallhead et al., 2014).

2.5. Bias-Corrected Projections Under SRES A1B Scenario (2001–2099)

For the projection run, atmospheric forcing was provided by a regional model system run by the Max Planck Institute, REMO (Keup-Thiel et al., 2006). This model was configured to cover the SINMOD domain (Figure 1) with a resolution of 0.22° and used output from the MPI-ECHAM5 coupled climate model system. Atmospheric CO_2 followed a climatological seasonal cycle from OWSM (66°N, 2°E) plus an ensemble-mean climatic trend under the SRES A1B scenario. Riverine inputs and tides were the same as in the hindcast run (see section 2.2). Boundary seawater fluxes were as for the hindcast run and biogeochemical boundary conditions were derived from monthly mean BCM projections with bias corrections as for the hindcast run. These projections were under the SRES scenario A2 rather than A1B, but this discrepancy should be small given the closeness of the atmospheric projections over our focus interval of the next 50 years (IPCC, 2000). SINMOD was initialized with the hindcast output for the year 2000 and run for years 2001–2099 inclusive under the A1B scenario, calculating CO_2 chemistry variables as described in section 2.2.

Bias-correcting climate model projections should be done with caution (Stock et al., 2011). We consider it justified here because our corrections are based on a hindcast driven by reanalysis atmospheric forcing, and because we use observations from an extended time interval (25 years) that is comparable with the focus projection interval (50 years). The projections were corrected by subtracting the bias predicted by the kernel smoothing or spline functions (see section 2.4) from the biweekly model output. Temperatures were constrained by a minimum plausible freezing point (predicted from the water pressure and a maximum plausible salinity of 40 psu), and (S, DIC, Alk, saturation state) were constrained by a lower limit of zero. Annual and bidecadal averages were subsequently computed from these constrained bias-corrected projections. As we are focused on 50 year climatic changes, we mainly compared output for 2000–2019 versus 2050–2069, using output from the A1B scenario run (bias corrected where possible) to compute both bidecadal averages.

To project threshold years for the onset of $CaCO_3$ undersaturation, we first averaged the biweekly output time series over seasons, assuming that undersaturation on subseasonal time scales is likely tolerable by

most benthic biota. We then averaged within season over ±10 years for each year (e.g., for winter 2020, all winters between 2010 and 2029 inclusive) to remove unpredictable interannual (internal) variability, and for each year we recorded the maximum and minimum seasonal Ω. The onset of seasonal/perennial undersaturation was then defined as the last year for which the minimum/maximum seasonal Ω exceeded 1.

2.6. Direct Drivers of Projected Acidification

Changes in bottom pH and Ω_{ar} due to individual factors (DIC, Alk, T, S, and silicate, phosphate—without bias correction) were calculated by summing partial increments, approximated as Euler steps between annual-averages using CO2SYS.m, to obtain annual time series of cumulative change Δ(pH, Ω_{ar}) due to each factor at each grid point. Our approach is similar to that of Yamamoto et al. (2012) except that we do not further decompose the (DIC, Alk) changes by process. Comparing the sum of the climatic changes (2000–2019 versus 2050–2069) due to each factor with the total climatic change from biweekly (pH, Ω_{ar}) output gave an absolute approximation error of $<$0.001 pH units at all depths 50–500 m within the study region (supporting information Figure S3).

3. Results

3.1. Model Skill Assessment

3.1.1. Point-To-Point Skill

Considering model-data pairs from years 1984 to 2008 and depths 50–500 m within the study region, bottom temperature shows the best correlation ($r = 0.89$) although this partly reflects the wide regional range (−2 to 16°C); SINMOD has a regional warm bias of 1.1°C and an RMS temperature error of 1.9°C (Figure 2a). SINMOD salinity is correlated with the observations ($r = 0.59$) but there is a clear bias, with SINMOD tending to exaggerate freshening in coastal low-salinity areas (cf. solid black regression line versus dashed 1:1 line in Figure 2b). Model-data correlations for bottom nitrate and silicate are lower ($r = 0.33$, 0.19) and there is a tendency to overestimate nitrate and underestimate silicate (Figures 2c and 2d). SINMOD bottom DIC and Alk are in reasonable agreement with observations although there is clearly too little variability in the model

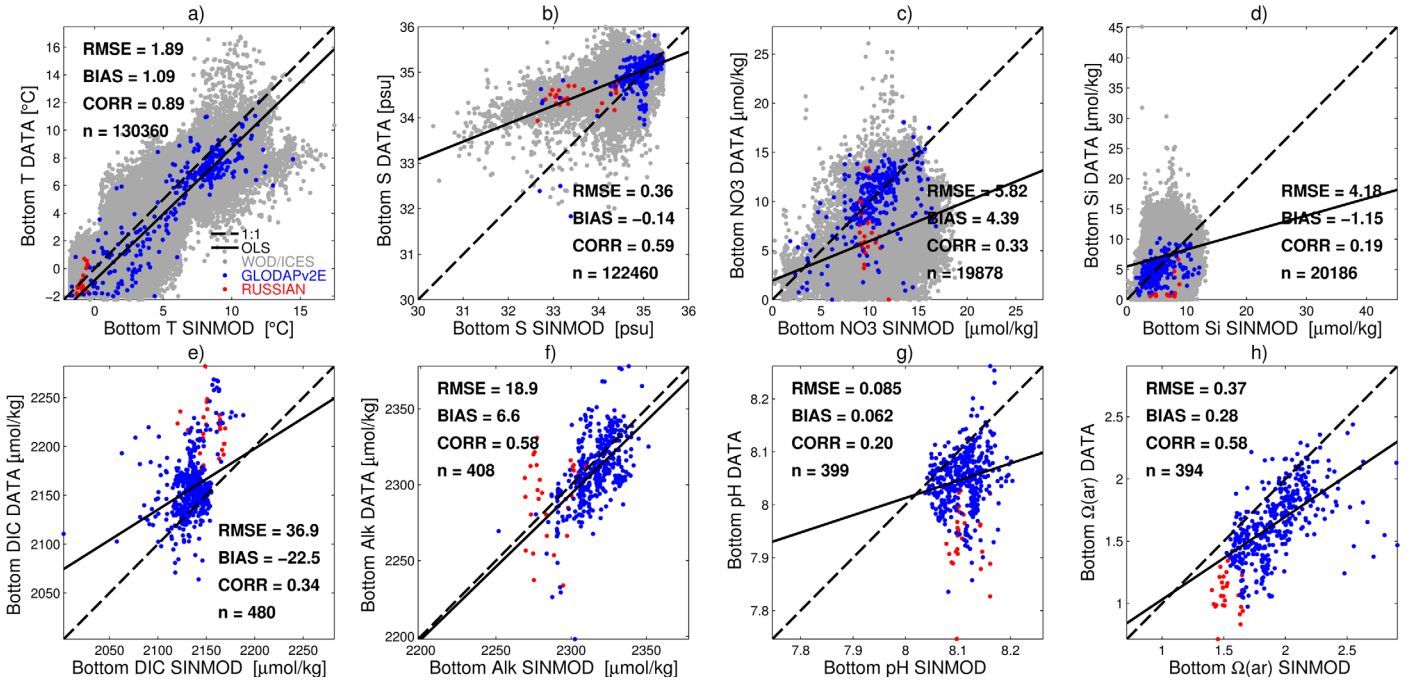

Figure 2. Point-to-point skill assessment for SINMOD bottom water variables. (a) T = temperature, (b) S = salinity, (c) NO3 = nitrate, (d) Si = silicate, (e) DIC = dissolved inorganic carbon, (f) Alk = total alkalinity, (g) pH = total-scale pH, and (h) Ω(ar) = aragonite saturation state. Modeled bottom water output was interpolated in 3-D (x,y,t) to the observational data, and skill was computed as RMSE = root-mean-square error, BIAS = mean(model-data), and CORR = Pearson correlation (n is the number of model-data pairs). Dashed black lines are 1:1, and solid black lines are from ordinary least squares linear regression. Data (points) are from WOD/ICES data sets (grey), the extended GLODAPv2 data set (blue), and the Russian Kara Sea data set (red).

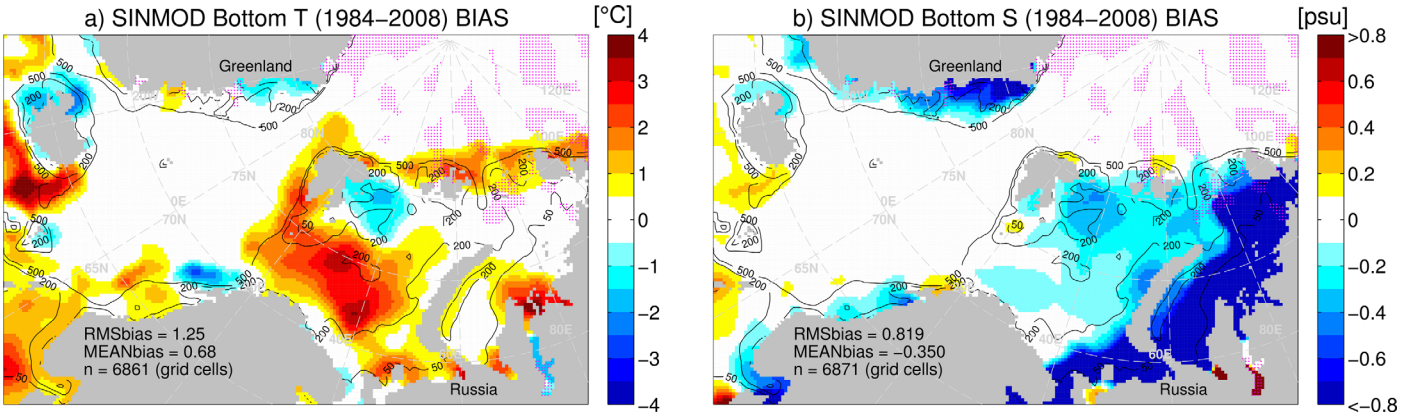

Figure 3. SINMOD regional biases in (a) bottom temperature and (b) bottom salinity. Magenta dots mark grid cells for which data coverage was lacking (no data within two bandwidths of the grid cell center). RMSbias and MEANbias show the root-mean-square and mean bias over all unmarked grid cells at model depths 50–500 m and "n" shows the number of such cells. Black lines show 50, 200, and 500 m depth contours.

(Figures 2e and 2f). Modeled total-scale pH is poorly correlated with the observations ($r = 0.20$) and shows too little variability (Figure 2g). Note, however, that this may primarily reflect the difficulty of simulating regional pH variations in the 50–500 m depth range, and does not necessarily reflect the accuracy of simulated climatic changes. The model-data correlation is better for aragonite saturation state Ω_{ar} ($r = 0.58$, Figure 2h). There is also a substantial negative bias in the modeled DIC (–22 μmol/kg) and positive biases in modeled pH (0.062) and Ω_{ar} (0.28).

3.1.2. Regional Biases

SINMOD bottom temperature show predominantly warm biases (mean = 0.68°C at depths 50–500 m) with hot spots reaching 3.5–4.0°C on, e.g., the central Barents shelf (Figure 3a). The salinity bias is predominantly fresh (mean = −0.35 psu) and mostly within –0.4 to 0.2 psu on the Norwegian and Barents shelves, but reaches high negative values (<–0.8 psu) in the shallower water of the East Greenland and Kara shelves (Figure 3b, cf. Figure 2b).

SINMOD DIC shows a negative bias that is largest at depths <50 m (magnitude >80 μmol/kg) but remains substantial (>10 μmol/kg) for depths 50–400 m (Figure 4a). By contrast, Alk bias is only substantial at depths <50 m (Figure 4b). We attribute the rapid increase in DIC/Alk bias at depths <50 m to the exaggerated coastal freshening (Figures 2b and 3b) while the broader-ranging DIC bias likely reflects missing remineralization fluxes at shallow-to-moderate depths (SINMOD bottom nitrate and silicate also show negative biases with respect to GLODAPv2E, although these are small relative to the error scatter, supporting information Figure S4). As a consequence of the imbalanced DIC/Alk biases, the SINMOD pH and Ω_{ar} are positively biased by 0.03–0.21 and 0.14–0.74 units, respectively, at depths 50–500 m (Figures 4c and 4d). Correcting these biases yields 5%–35% reductions in RMSE (cf. SINMOD versus SINMODub = "SINMOD unbiased" results in Figure 4) and improved consistency with observations in almost all subregions of the pan-Arctic domain (supporting information Figures S1 and S2).

3.1.3. Temporal Trend Model Skill Assessment

Observations show rapid warming trends of 0.3–0.6°C/decade at IRM and OWSM (Figures 5a and 5m), and salinization trends of 0.02–0.06 psu/decade at IRM over 25 years (Figure 5b). These are not reproduced by the SINMOD hindcast (see red lines and crosses). However, the observations also show increasing trends in DIC (4–10 μmol/kg/decade) and pCO_2 (10–25 μatm/decade) at both IRM and IS stations over the 14–18 sampled years (Figures 5c, 5d, 5i, and 5j). SINMOD approximately reproduces these trends at depths ≤200 m; deeper down there are incorrect decreasing trends, suggesting an inadequate spin-up period or initial condition. Significant decreasing trends are observed in total-scale pH (0.015–0.025 per decade, Figures 5e and 5k) and aragonite saturation state at IS at depths ≥200 m (0.01–0.02 per decade, Figure 5l). Again, SINMOD trends are broadly consistent with observations for depths ≤200 m, although at IRM the SINMOD trends at 100 and 200 m appear to be slightly exaggerated (Figures 5e and 5f).

At OWSM, there was insufficient data coverage to assess the uncertainty in observational trend estimates for CO_2 chemistry variables. Instead we show analyses for the Kola time series stations in the southern

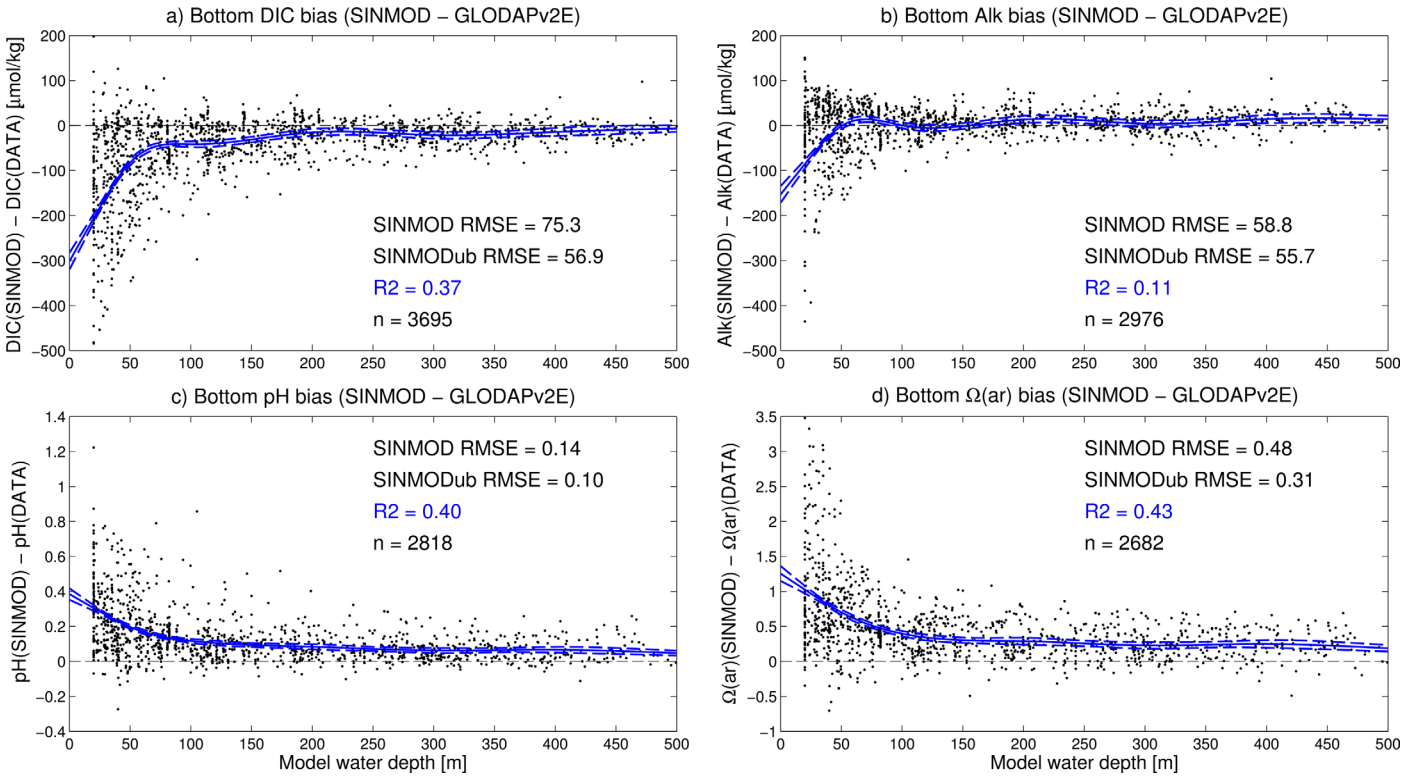

Figure 4. SINMOD regional bottom water biases for (a) dissolved inorganic carbon, (b) total alkalinity, (c) total-scale pH, and (d) aragonite saturation state . Black dots show model-data errors for all GLODAPv2-extended data within the SINMOD pan-Arctic domain and within the test period 1984–2008. Blue lines show fitted spline bias functions (dashed lines are 95% CIs). Statistics in plots show the reduction in RMSE achieved by the bias-corrected model ("SINMODub") as well as the R-squared values (R2) and sample sizes (n) for the bias function fits.

Barents Sea, where temperature observations were available for all years within the test period (Figures 5o–5q). Despite the good data coverage, the trends at these stations are highly uncertain due to the strong decadal-scale variability in these time series, which is well reproduced by SINMOD (e.g., supporting information Figure S5). Nevertheless there is marginal evidence that the SINMOD warming trends are also too weak at these stations (Figures 5o–5q).

3.2. Model Projections Under SRES A1B Scenario

3.2.1. Fifty Year Changes in Bottom Water Environment

Comparisons of SINMOD bottom temperature during years 2000–2019 and 2050–2069 inclusive shows a median warming of 1.5°C at depths 50–500 m (Figures 6a–6c). However, spatial variability is high (2.5%–97.5% quantiles are 0.1–2.7°C) and warming >2.75°C is observed in the shallows of the northern and eastern Barents Sea (Figure 6c). The same areas also undergo salinization (Figure 6f), suggesting a northward/eastward intrusion of Atlantic water, pushing back the cooler and fresher Arctic water. The largest bottom salinity increases (∼1.4 psu) occur in the Kara Sea, in shallow water (<50 m) adjacent to large salinity decreases in deeper water further from the Russian coast (Figure 6f). Horizontal-depth transects suggest that this reflects the displacement of surface, low-salinity coastal water by saltier oceanic water (not shown). The freshening of deeper water is here associated with a decrease in ice cover of 100–150 days per year (Figure 7c) and a 25%–50% increase in annual mixed layer depth (Figure 7f); the increased surface exposure may thus have freshened the bottom water by promoting wind-driven vertical mixing with the fresher surface water. The largest relative increases in vertical mixing occur in the northern Barents Sea (Figure 7e), but here the ice loss is almost complete (Figure 7b), so the "Atlantification" effect dominates and bottom salinity increases. Bottom freshening reaching −1.5 psu occurs on the western Russian and East Greenland shelves (Figure 6f), and is also associated with loss of ice cover (Figure 7c). Here the surface layers freshen (not shown) and mixed layer depth changes are small or negative (Figure 7f), suggesting that increased meltwater supply is the primary driver.

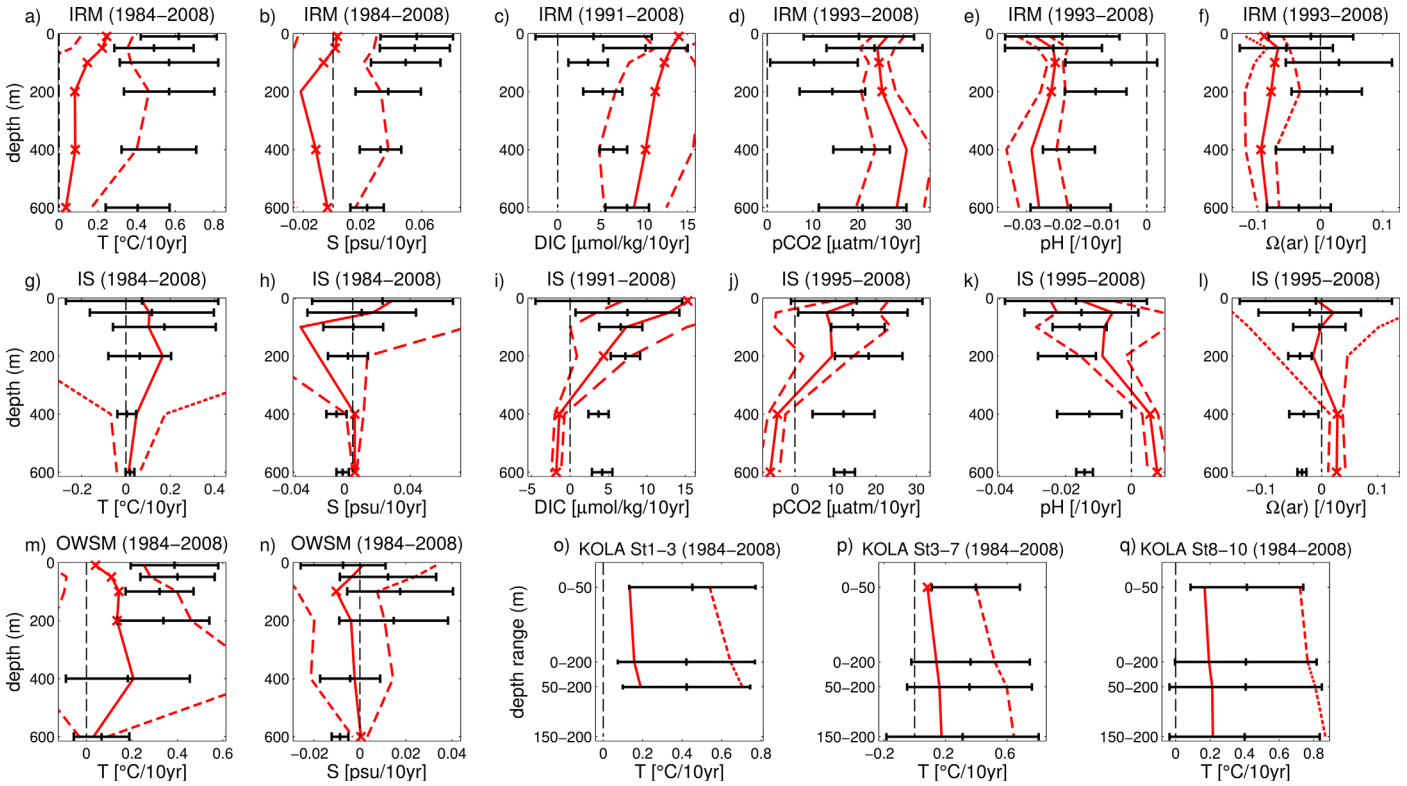

Figure 5. SINMOD temporal trend skill assessment. Subplots show results from four time series stations: (a–f) Irminger Sea (IRM), (g–l) Icelandic Sea (IS), (m, n) Ocean Weather Station M (OWSM), and (o–q) the Kola Section. Black error bars show observed trends ±95% CIs, red envelopes show SINMOD trends ±95% CIs, and red crosses identify depths where trends in model-data errors were significant ($p < 0.05$).

Bottom DIC increases rapidly at depths <500 m (Figures 8a–8c). On the Russian and East Greenland shelves, the penetration of anthropogenic CO_2 and North Atlantic alkalinity is counteracted by increasing freshwater input from ice melt and river discharge, which decreases Alk and mitigates the DIC increase (Figures 8c and 8f). Changes in bottom Alk correlate strongly with changes in salinity ($r = 0.92$ for depths 50–500 m within the study region, cf. Figures 7d–7f) and thus reflect the advance of Atlantic water and changes in vertical mixing and freshwater input discussed above, while the correlation of ΔDIC with ΔS is reduced by the invasion of atmospheric CO_2 ($r = 0.66$). Neither ΔDIC nor ΔAlk correlate with changes in primary productivity or vertical export ($|r| < 0.07$; supporting information Figures S6c and S6f), suggesting that the modeled biological amplification of bottom water acidification (sensu Bates & Mathis, 2009) is a weak effect in this region. This is further confirmed by the changes in bottom nitrate and silicate concentrations (supporting information Figure S7), which do not show increases corresponding to the increases in productivity and export at the frontier of ice retreat (supporting information Figure S6).

The resulting changes in total-scale bottom pH show rapid and spatially variable acidification in the study region, with bidecadal averages at depths 50–500 m decreasing by 0.10–0.20 units (2.5%–97.5% quantiles, median = 0.16) (Figure 9c). Both present and future values of bottom Ω_{ar} show undersaturation ($\Omega_{ar} < 1$) in the deep basins and in the Kara Sea (Figures 9d and 9e), but the future period also shows undersaturation on the northern/eastern Barents and East Greenland shelves (Figure 9e). The decrease in Ω_{ar} at 50–500 m is 0.26–0.57 units (2.5%–97.5% quantiles, median = 0.40) (Figure 9f).

Threshold years show a similar progression whether we consider seasonal or perennial undersaturation, due to the generally weak seasonality in bottom water variables (Figure 10 versus supporting information Figure S8). For aragonite, already by 2020 there is seasonal undersaturation over most of the Kara Sea as well as in the deep basins (Figure 10a). By 2040, the undersaturation has spread to the deeper Kara Sea as well as the shallower parts (mostly <200 m) of the northern/eastern Barents and East Greenland shelves. By 2070 most of the Barents and East Greenland shelf bottom water is undersaturated with respect to Ω_{ar}. The

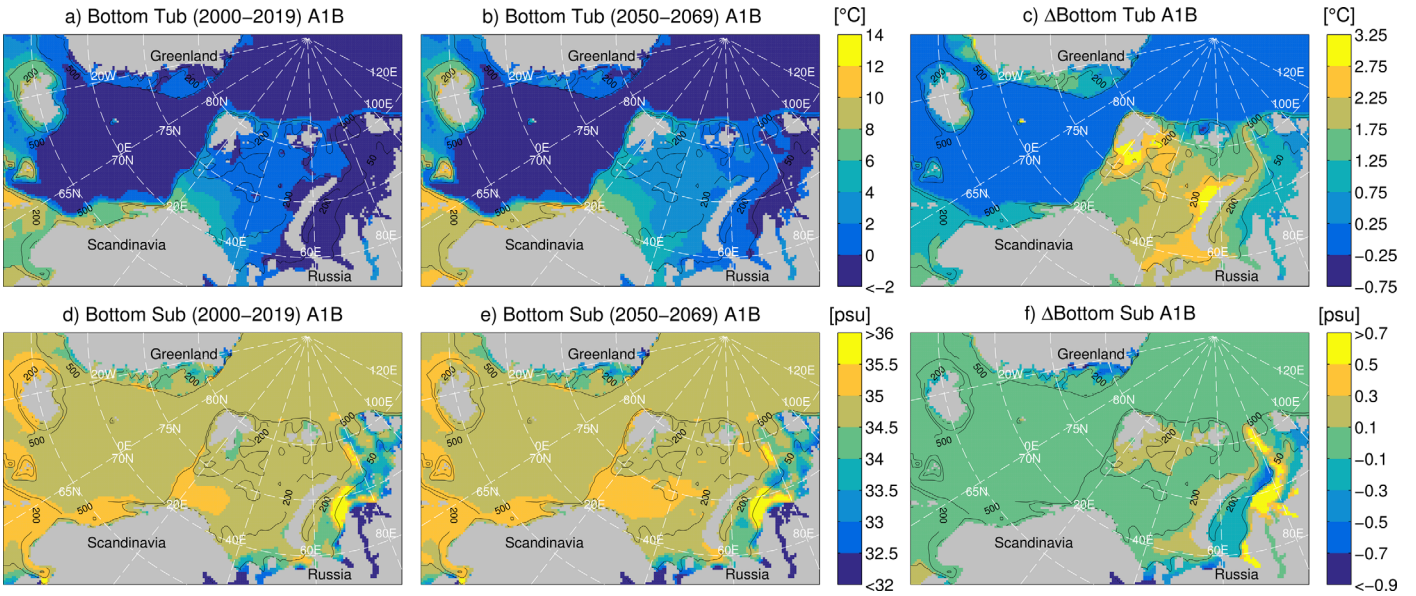

Figure 6. Bias-corrected SINMOD projections for (top) bottom temperature and (bottom) salinity under SRES A1B scenario. Left and middle plots show bidecadal averages over (2000–2019) and (2050–2069), respectively, and right plots show the differences. Black lines show 50, 200, and 500 m depth contours.

south-western Barents Sea and the Norwegian shelf down to 500 m depth become seasonally undersaturated with respect to Ω_{ar} during 2070–2090, although some shallower parts avoid perennial undersaturation before 2090 (supporting information Figure S8a). Bottom water undersaturation with respect to calcite before 2090 and within the study region is confined to the Kara Sea and East Greenland shelf at depths $<$200 m, plus the deep Eurasian Basin (Figure 10b). Very similar results are obtained using monthly average rather than season-average model output (supporting information Figures S9 and S10). Projections for south of Iceland and at depths $>$500 m are treated with caution as they may be affected by problems with the initial condition/spin-up (see section 3.1.3).

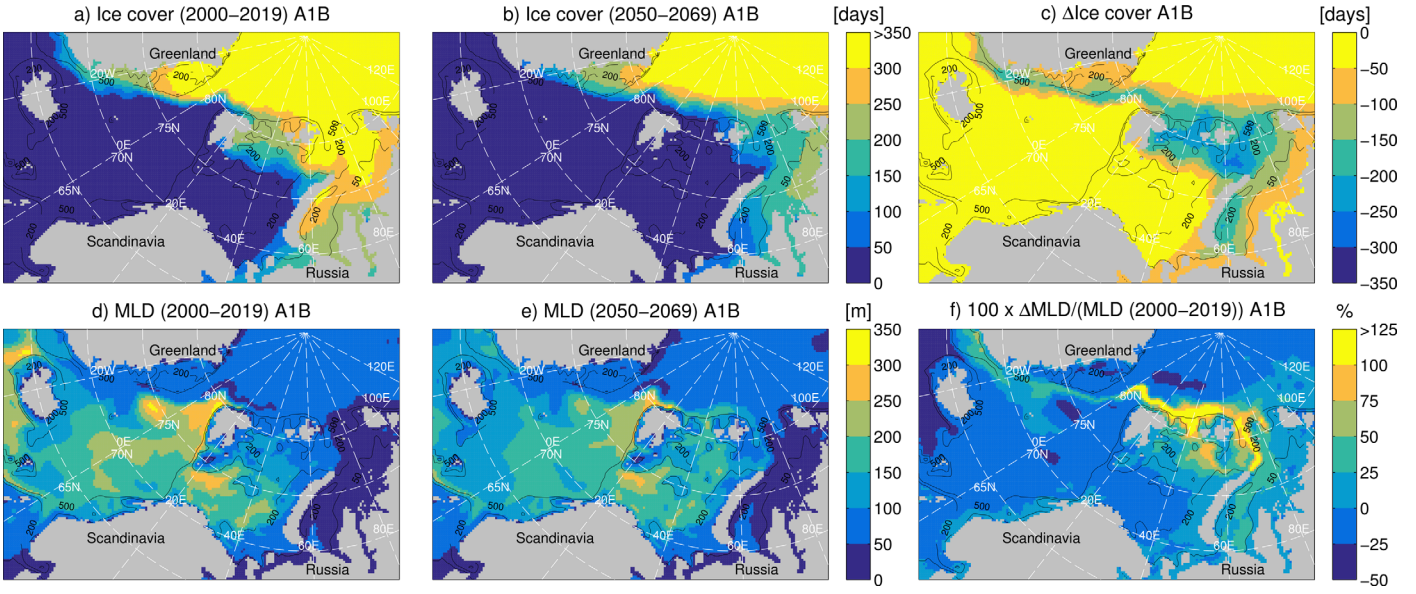

Figure 7. SINMOD projections for (top) ice cover (number of days with nonzero ice thickness) and (bottom) mixed layer depth under the SRES A1B scenario. Left and middle plots show bidecadal averages over (2000–2019) and (2050–2069), respectively, and right plots show the differences. For mixed layer depth, the differences (f) are expressed as percentages of the (2000–2019) averages. Black lines show 50, 200, and 500 m depth contours.

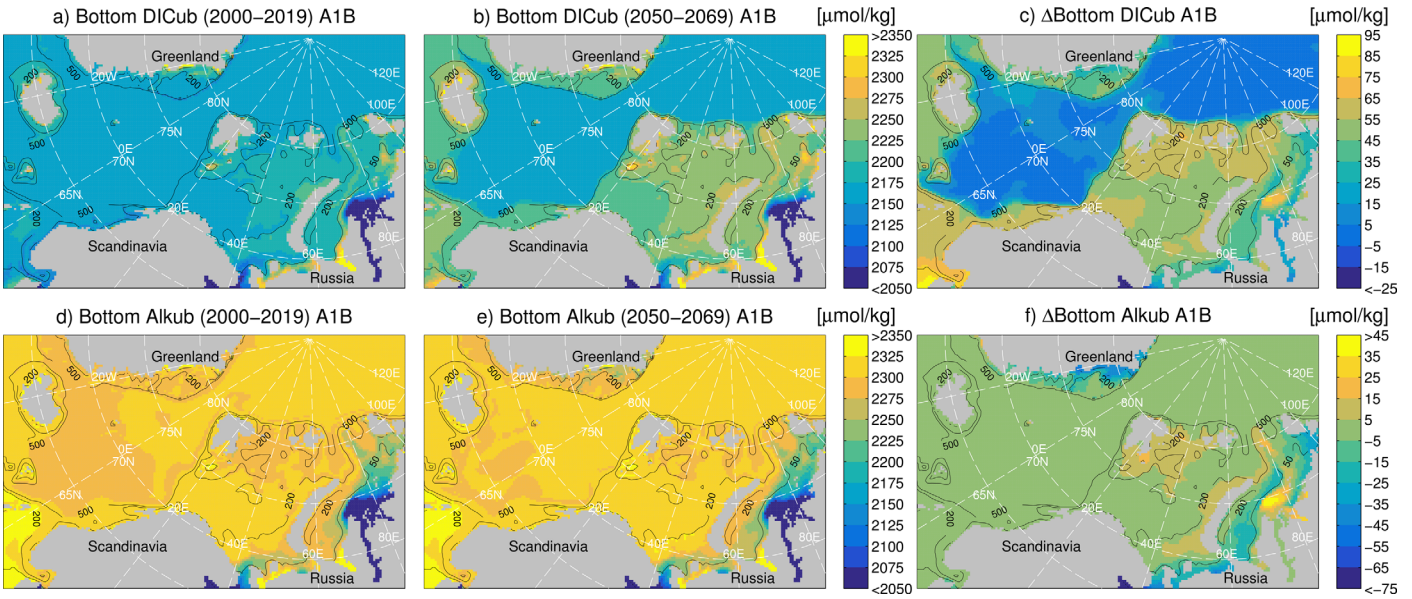

Figure 8. Bias-corrected SINMOD projections for (top) bottom dissolved inorganic carbon and (bottom) total alkalinity under the SRES A1B scenario. Left and middle plots show bidecadal averages over (2000–2019) and (2050–2069), respectively, and right plots show the differences. Black lines show 50, 200, and 500 m depth contours.

3.2.2. Direct Drivers of Shelf Bottom Acidification

From the attribution analysis, changes due to DIC increase emerge as clearly dominant and account for most of the pH reduction on the Norwegian and Barents shelves (Figure 11a). On the Russian and East Greenland shelves, freshening reduces the contribution of DIC (Figure 11a), but this is compensated by corresponding reductions in Alk (Figure 11b). Similarly, the buffering effect of increased Alk in the northern Barents Sea (Figure 11b) is compensated by a larger input of DIC from the advancing Atlantic water (Figure 11a), and the large freshening-driven changes due to DIC and Alk in the Kara Sea also largely compensate each other. Exacerbation by warming is important in the Barents Sea, where it accounts for an additional

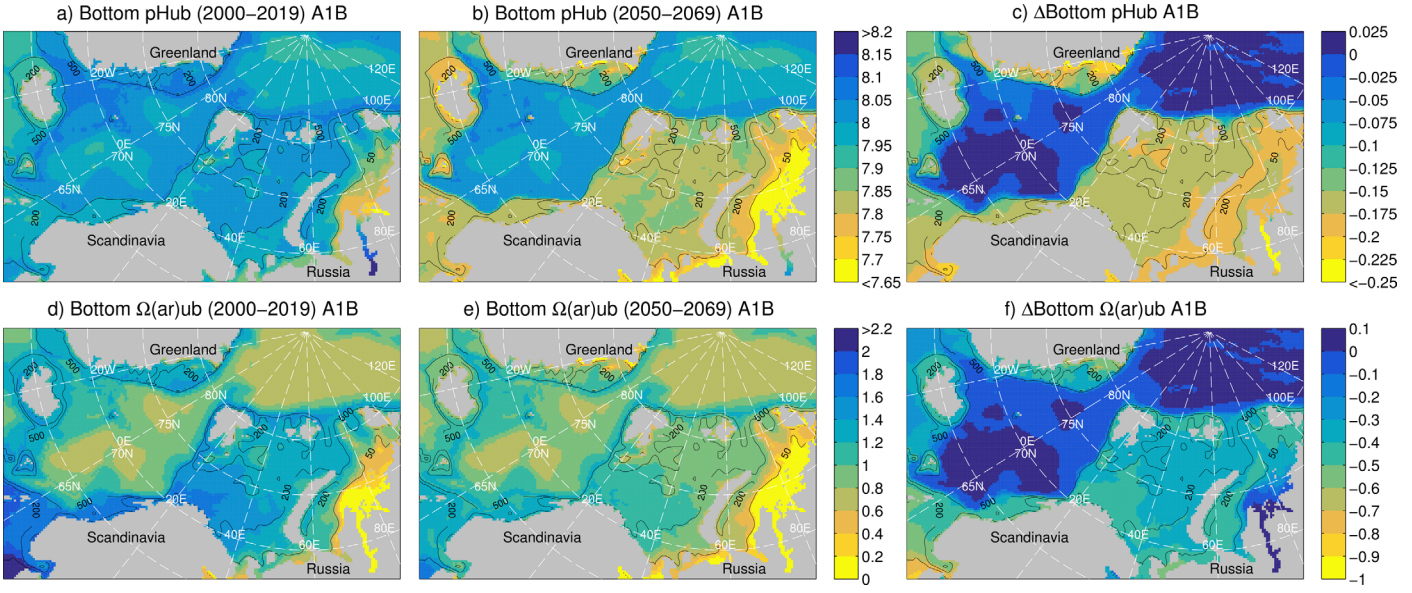

Figure 9. Bias-corrected SINMOD projections for (top) bottom pH and (bottom) aragonite saturation state under the SRES A1B scenario. Left and middle plots show bidecadal averages over (2000–2019) and (2050–2069), respectively, and right plots show the differences. Black lines show 50, 200, and 500 m depth contours.

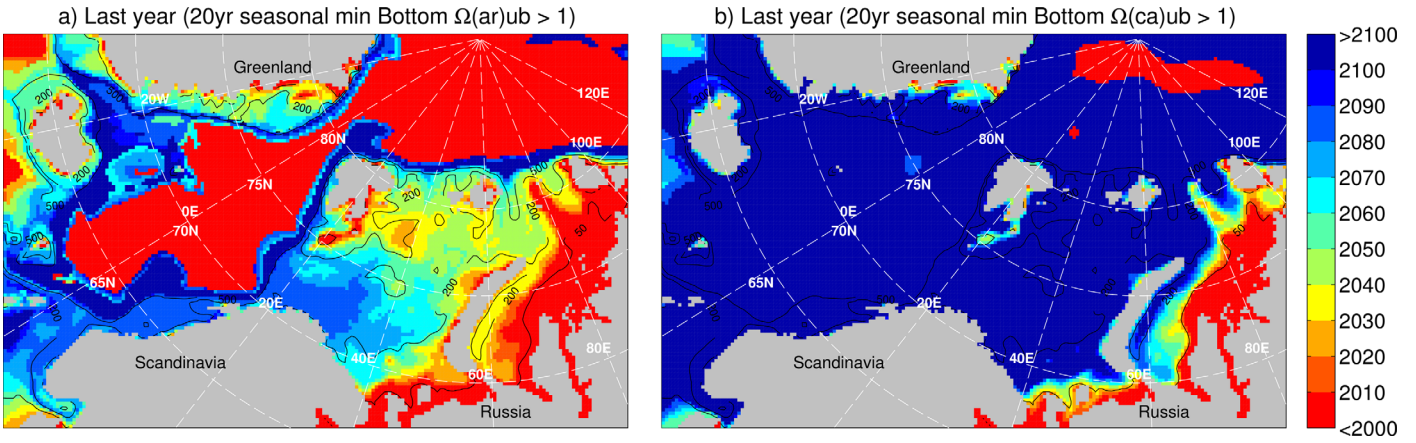

Figure 10. Threshold years for the onset of seasonal bottom water undersaturation with respect to (a) aragonite and (b) calcite. Colors show the last years for which the climatic (20 year moving average) seasonal minimum bottom saturation state is >1. Black lines show 50, 200, and 500 m depth contours.

0.03 pH units decrease on average (Figure 11c). The effect of salinity changes per se, i.e., through changes in CO_2 system equilibrium constants, is generally insignificant, as are the effects of changes in silicate and phosphate concentrations (supporting information Figure S11). A similar pattern of attribution applies to the changes in bottom Ω_{ar} except that here the contributions of warming are also negligible (supporting information Figure S12).

We note that mixing with freshwater can influence pH and Ω_{ar}, depending on the DIC/Alk of the freshwater and whether equilibration with atmospheric pCO_2 is assumed. However, for the largest salinity changes observed in the bottom water projections at 50–500 m (~1 psu within 30–35 psu), the impacts of freshwater mixing are small for all relevant mixing conditions ($|\Delta pH| < 0.01$, $|\Delta\Omega_{ar}| < 0.1$, see supporting information Figure S13).

4. Discussion

4.1. Comparison With Other Projections

While a detailed model intercomparison is beyond our scope, we provide here a brief comparison with other climate and ocean acidification projections for the study area. These are somewhat limited by the tendency of studies to focus on surface rather than bottom water projections. Considering downscaling models, Skogen et al. (2014) used a ROMS-NORWECOM model to project an Ω_{ar} decrease of 0.4–0.8 units on the Norwegian shelf at 50–500 m between 1998–2000 and 2063–2065 under SRES A1B (from their Figure 9). For the same periods and region, SINMOD projects a similar range of decreases (0.3–0.7 units) despite using different forcings, boundary conditions, and physical/biogeochemical model components. Sandø et al. (2014) report bottom water warming of 1–2°C and up to 4°C in the Barents Sea for two ROMS downscaling models, comparing 1981–2000 versus 2046–2065 under SRES A1B. Between these periods, for the Barents Sea (70°N–80°N, 20°E–50°E), SINMOD projects bottom warming of 1.8–4.3°C (cf. Figure 6c).

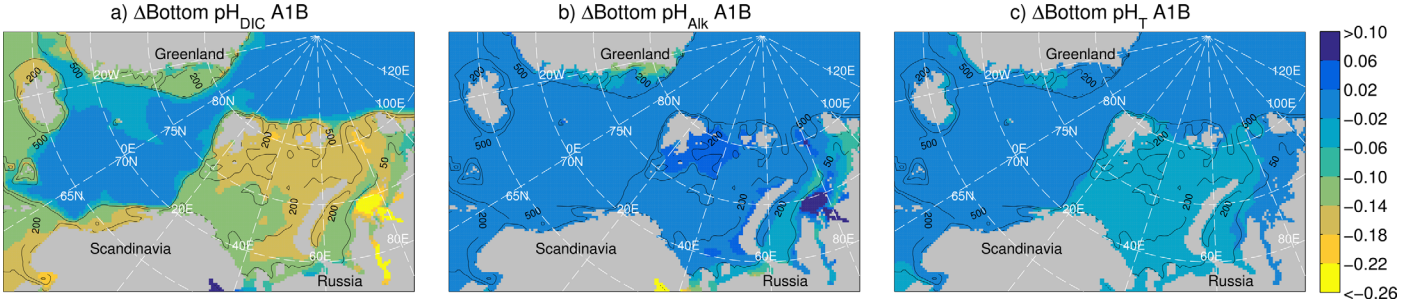

Figure 11. Direct drivers of climatic changes in bottom pH. Subplots show changes in bottom water pH between (2000–2019) and (2050–2069) under SRES A1B scenario due to changes in (a) dissolved inorganic carbon, (b) total alkalinity, and (c) temperature. Black lines show 50, 200, and 500 m depth contours.

Considering global models, Steinacher et al. (2009) used NCAR CSM1.4 to project a mean decrease in annual surface Ω_{ar} of 0.5 units for latitudes >70°N between surface atmospheric CO_2 concentrations of 390 and 560 ppm, corresponding to our time periods 2000–2019 and 2050–2069 under SRES A1B (see their Figure 7a). For the same region and periods, SINMOD mean surface Ω_{ar} decreases by 0.51 units. Similarly, Yamamoto et al. (2012) report mean decreases in Arctic surface pH of 0.18–0.19 and surface Ω_{ar} decreases of 0.40–0.57 between 390 and 560 ppm, considering two versions of MIROC-ESM and all ice-influenced regions north of 65°N (see their Figure 5). SINMOD projects corresponding mean pH and Ω_{ar} decreases of 0.22 and 0.53, respectively. Popova et al. (2014) used a global NEMO-MEDUSA model to project the spread of undersaturation in the shelf bottom water, and their results are quite consistent with our Figures 10a and 10b (cf. their Figures 6d and 6c). Meehl et al. (2007) report an ensemble mean warming of 0.5–1.5°C at depths 50–500 m and latitudes >70°N between periods (1980–1999) and (2046–2065) under SRES A1B (their Figure 10.7b). Corresponding SINMOD average warming is 1.1°C at 50 m and 0.6°C at 500 m.

The SINMOD-projected bottom acidification can also be compared with a simple downward extrapolation of the change in atmospheric pCO_2 over the next 50 years (supporting information Figure S14). Under the SRES A1B scenario, atmospheric pCO_2 increases by 171 μatm between 2000–2019 and 2050–2069. Considering the increase in SINMOD bottom pCO_2 in all grid cells at depths 50–500 m within the study region, the median value is 190 μatm, only 11% higher than the extrapolation projection. However, spatial variability is significant (2.5–97.5% quantiles are 98–217 μatm) and suggests a limited value of the extrapolation method for making local-scale projections.

Our attribution analysis (section 3.2.2) showed that the primary direct driver of bottom water acidification on the shelves is the accumulation of anthropogenic DIC, with secondary roles played by alkalinity reductions and warming. This is consistent with previous analyses of surface changes (Popova et al., 2014; Steinacher et al., 2009; Yamamoto et al., 2012) except that for bottom water deeper than 50 m, the direct impacts of freshwater mixing are small (supporting information Figures S13d and S13f; cf. Azetsu-Scott et al. 2010, Figure 10b; Denman et al., 2011, Figure 4; and Tank et al., 2012, Figure 8). Note, however, that our analyses only consider direct effects; the modeled accumulation of bottom DIC may itself be sensitive to ocean warming and freshening, via associated changes in circulation, mixing, ice cover, CO_2 uptake, and biological response, as well as the freshwater-borne fluxes of DIC and Alk from land-derived sources (Popova et al., 2014; Steinacher et al., 2009; Yamamoto et al., 2012).

4.2. Uncertainties in the Downscaling Projections

In our view, a full assessment of our projection uncertainties would require an ensemble of projections from downscaling ocean biogeochemical models (and/or high-resolution global models, Holt et al., 2017) because the extra spatial resolution can correct large biases in stratification and horizontal transport (Ådlandsvik, 2008; Melsom et al., 2009; Sandø et al., 2014). We also suggest that for impact studies, the projections should be corrected for bias both in the model inputs and in the outputs, as long as this can be robustly estimated, because some stressors (e.g., Ω) may depend strongly on absolute values as well as the climatic changes (cf. Ciais et al., 2013, Figure 6.28). Although such an ensemble is not yet available to us, it is useful to consider here the main sources of uncertainty and implications of our skill analyses (section 3.1) and comparisons with other projections (section 4.1).

Boundary conditions are potentially major sources of projection uncertainty for downscaling models. We tested the sensitivity of bottom pH projections by rerunning the model with the North Atlantic boundary conditions fixed as climatological seasonal cycles based on the CARINA data set. The pH decrease on the Norwegian shelf was reduced by around 0.05 units but the acidification of Barents, Kara, and East Greenland shelves was largely unchanged (supporting information Figures S15a and S15b), mainly because the reduced horizontal input of CO_2 from northward flowing currents was compensated by increased vertical input via air-sea gas exchange (Figures S15c and S15d). Similar results are obtained for temperature, with only ∼0.5°C and ∼0.25°C reductions in the warming on the Norwegian and Barents shelves, respectively (supporting information Figure S16). This suggests that errors in boundary conditions are unlikely to have strongly exaggerated our acidification and warming projections on the northernmost shelves.

Other typical sources of uncertainty include the structure and parameterization of the ice and biological model components and their response to errors in the atmospheric forcing (Slagstad et al., 2015). However, within our study region, the projected changes in ice cover and vertical mixing (Figures 7c and 7f) and

primary production and particulate export (supporting information Figures S6c and S6f) did not show strong correlations with the bottom water warming or acidification ($|r| < 0.35$, cf. Figures 6c, 9c, and 9f) and any consequent freshening of the bottom water (Figure 6f) was too weak at depths >50 m to have a strong impact on pH or saturation state (supporting information Figures S11–S13). This raises the prospect that the projected bottom acidification/warming at depths >50 m may be somewhat robust to the uncertainties in ice dynamics, stratification, and biological response that are typically large on climatic time scales and which may strongly influence surface properties, including primary productivity (Artioli et al., 2014; Denman et al., 2011; Popova et al., 2010; Vancoppenolle et al., 2013; Yool et al., 2015) and surface acidification (Artioli et al., 2014; Popova et al., 2014; Steiner et al., 2014).

Caution is required here regarding the biological response and potential "biological amplification" of bottom water OA (Bates & Mathis, 2009). Comparisons by Wassmann et al. (2006) with short-term sediment trap observations from the central Barents Sea (Olli et al., 2002) suggested a tendency for SINMOD to underestimate particulate carbon export fluxes, which may partly explain the negative bias in bottom DIC over the pan-Arctic shelves (Figure 4a). Also, the formulation of benthic remineralization is rather simple (see section 2.1), the elemental stoichiometry of biogeochemical processes is fixed, the model neglects brine transport and potential fractionation of DIC versus Alk during ice formation (Rysgaard et al., 2007; Loose et al., 2011; Bellerby et al., 2013), ice algae are not explicitly represented, warming responses (e.g., through Q10 values, see Wassmann et al., 2006) are uncertain, and there is currently no sensitivity of (planktonic) biological processes to OA (e.g., Artioli et al., 2014; Heinze, 2004; Oschlies et al., 2008; Riebesell et al., 2007; Schneider et al., 2004). If these processes are subject to strong climatic change then our static bias corrections may have failed to compensate the errors in the projections. Climatic changes in the riverine inputs have also been neglected and could also bias our projections, especially if they include organic matter inputs that degrade slowly and thus impact seawater chemistry far beyond the coast (Manizza et al., 2011). In particular, projections for the Russian shelves (including the Kara shelf) could be strongly affected by biases in riverine inputs and benthic remineralization fluxes (Anderson et al., 2011; Semiletov et al., 2016).

Another concern is the model spatial resolution, here 20 km in the horizontal. One might ask whether an eddy-resolved model (which may require <1 km resolution at these latitudes, Holt et al., 2014) could result in similar biases relative to 20 km models as between 20 km models and present global climate models. We tentatively expect this not to be the case within our study region, in oceanic water deeper than 50 m, because the 20 km resolution appears to be sufficient to resolve the primary northward inflow current (the Norwegian Atlantic Current) and the primary southward outflow current (the East Greenland Current) (Slagstad et al., 2015). The present resolution is not sufficient to resolve mesoscale eddies or shallow-water coastal currents such as the Norwegian Coastal Current. However, comparisons of primary productivity between the original 20 km model (Slagstad & Wassmann, 1996) and a later 4 km version (Wassmann et al., 2006) have shown only a minor increase (~15%) and a similar spatial distribution (Slagstad et al., 2015). The failure of our hindcast to capture recent warming/salinization trends (Figures 5a, 5b, 5m, and 5p) does not, we believe, reflect inadequate resolution of northward currents in SINMOD, but rather a lack a recent warming trend in the driving BCM boundary condition, which was based on a "historical" simulation with likely the wrong phase of decadal-scale variability. We hope to test this hypothesis in future work using boundary conditions for the hindcast run based on reanalysis data.

Regarding vertical resolution, we note that the present SINMOD vertical grid (see section 2.1) was, like most models, not specifically designed to resolved bottom water variability. Indeed, the Barents Sea warm biases shown in Figure 3a may be due to the fixed z-levels with thickness 100–200 at 500 m depth causing excessive heating of the bottom water by shelf inflow currents. It is not clear whether a terrain-following vertical grid will necessarily improve matters; while this can improve warming and stratification responses in shallow water (Ådlandsvik, 2008), it can also lead to spurious diapycnal mixing in regions of steep shelf topography (Marchesiello et al., 2009).

Further simulations are needed to address all these uncertainties, and the skill assessment of the present model (Figures 2–5) shows that there is plenty of scope for improvement in both physical and biogeochemical components. A key requirement for the continued improvement of model projections is the availability of quality-controlled observational data for model skill assessment, bias correction, and eventually weighting factors for multimodel projections (Tebaldi & Knutti, 2007). A challenge here is that much of the historical CO_2 chemistry observations from the Russian shelves, which may be bellwethers of broader-scale

acidification (Figure 10), are derived from methods that do not conform to international standards. Same-sample inter-laboratory comparisons are needed to assess possible biases in these Russian data; in the meantime, we can report that the bias correction of the SINMOD output, based on an independent data set subjected to stringent quality control (GLODAPv2E), did substantially reduce the bias with respect to the Russian bottom water observations at depths 50–500 m (from 0.175 to 0.072 for pH, from 0.45 to 0.10 for Ω_{ar}), suggesting that the disagreement (see red dots in Figures 2g and 2h) may largely reflect model bias in the shallow Kara Sea.

5. Conclusions

We used a downscaling ocean biogeochemical model of moderate complexity to investigate shelf bottom climate change in the western Eurasian Arctic region. A hindcast was run to assess model skill, bias, and climatic trends, and bias-corrected projections were analyzed for the present century under a business-as-usual scenario, with a focus on the next 50 years and on bottom water at depths between 50 and 500 m.

The projections showed rapid and spatially variable shelf bottom acidification by 0.10–0.20 pH units over 50 years (2.5%–97.5% quantiles). This corresponds to a further 26%–58% increase in the hydrogen ion concentration, on top of the ~26% increase that has likely already occurred since preindustrial times. Bottom water undersaturated with respect to aragonite is simulated for the present day in the shallow Kara Sea; under the business-as-usual scenario this corrosive area grows to cover the entire Kara shelf by 2040 and most of the Barents and East Greenland shelves by 2070. The acidification is combined with highly variable warming of 0.1–2.7°C over 50 years (2.5%–97.5% quantiles). This could act as a multistressor, especially in northern and eastern parts of the Barents shelf. The accumulation of anthropogenic CO_2 was identified as the dominant driver of shelf acidification, consistent with previous analyses and the weak projected freshening of the bottom water at depths >50 m.

Although we were unable to validate the warming and deep acidification trends in the model hindcast, we believe this was mainly due to issues with the hindcast model inputs, which should have little effect on the projections. The model did successfully reproduce observed shallow acidification trends, and the basin-scale agreement between SINMOD and other models, using different grid structure/resolution and different ice/biological model formulations, suggests that these sources of uncertainty have limited impact on basin-scale projections, at least in regard to acidification. However, a robust uncertainty assessment at regional and local scales is likely to require an ensemble of downscaling or high-resolution global models for this region.

Projecting environmental change in the ocean is a challenging and multifaceted problem that requires a team effort across scientific disciplines and between modelers, observationalists, and data analysts. For the Arctic Ocean, it is clear that an international effort is needed, and if we want to understand the potential future impacts of acidification in American and Nordic/European sectors, we would likely do well to study the present state and historical changes on the Russian shelves. In future work, we will aim to combine the bottom water environmental information from the model with benthic species presence/absence data, in order to investigate and project future impacts on benthic species distributions.

Acknowledgments
We gratefully acknowledge financial support from: the Polish-Norwegian Research Program, operated by the National Centre for Research and Development under the Norwegian Financial Mechanism 2009–2014 in the frame of Project Contract Pol-Nor/196260/81/2013 (P.W., R.B.); the FRAM High North Research Centre for Climate and the Environment under the project ECOAN (P.W.); the Norwegian Research Council under projects MERCLIM (184860, R.B., A.S., D.S.) and MICROPOLAR (225956/E10, P.W., R.B.); the State Key Laboratory for Estuarine and Coastal Research under projects VOCO and Foreign Experts (R.B.); and the European Union Seventh Framework Program (FP7/2007–2013) under projects MEECE (212085) and EURO-BASIN (26493) (R.B.). We also thank the journal Editor and two anonymous reviewers whose constructive criticism has greatly helped to improve the manuscript. Data including bottom water observations and bias-corrected model output are openly accessible at Zenodo (https://doi.org/10.5281/zenodo.886077).

References

Ådlandsvik, B. (2008). Marine downscaling of a future climate scenario for the North Sea. *Tellus Series A*, *60*(3), 451–458. https://doi.org/10.1111/j.1600-0870.2008.00311.x

Ådlandsvik, B., & Bentsen, M. (2007). Downscaling a twentieth century global climate simulation to the North Sea. *Ocean Dynamics*, *57*(4–5), 453–466. https://doi.org/10.1007/s10236-007-0125-2

Amon, R. M. W., & Meon, B. (2004). The biogeochemistry of dissolved organic matter and nutrients in two large Arctic estuaries and potential implications for our understanding of the Arctic Ocean system B. *Marine Chemistry*, *92*, 311–330. https://doi.org/10.1016/j.marchem.2004.06.034

Anderson, L. G., Björk, G., Jutterström, S., Pipko, I., Shakhova, N., & Wåhlstöm, I. (2011). East Siberian Sea, an Arctic region of very high biogeochemical activity. *Biogeochemistry*, *8*, 1745–1754. https://doi.org/10.5194/bg-8-1745-2011

Anthony, K. R. N., Kleypas, J. A., & Gattuso, J. P. (2011). Coral reefs modify their seawater carbon chemistry—Implications for impacts of ocean acidification. *Global Change Biology*, *17*, 3655–3666. https://doi.org/10.1111/j.1365-2486.2011.02510.x

Artioli, Y., Blackford, J. C., Nondal, G., Bellerby, R. G. J., Wakelin, S. L., Holt, J. T., . . . Allen, J. I. (2014). Heterogeneity of impacts of high CO_2 on the North Western European Shelf. *Biogeosciences*, *11*(3), 601–612. https://doi.org/10.5194/bg-11-601-2014

Azetsu-Scott, K., Clarke, A., Falkner, K., Hamilton, J., Jones, E. P., Lee, C., . . . Yeats, P. (2010). Calcium carbonate saturation states in the waters of the Canadian Arctic Archipelago and the Labrador Sea. *Journal of Geophysical Research*, *115*, C11021. https://doi.org/10.1029/2009JC005917

Bates, N. R., & Mathis, J. T. (2009). The Arctic Ocean marine carbon cycle: Evaluation of air-sea CO2 exchanges, ocean acidification impacts and potential feedbacks. *Biogeosciences*, *6*, 2433–2459.

Bellerby, R., Anderson, L., Azetsu-Scott, G., Croot, K., Macdonald, P. R., Miller, L., . . . Steiner, N. (2013). Acidification in the Arctic Ocean. In *Arctic Ocean acidification* (pp. 9–33). Oslo, Norway: Arctic Monitoring and Assessment Programme.

Bellerby, R. G. J., Olsen, A., Furevik, T., & Anderson, L. G. (2005). Response of the surface ocean CO_2 system in the Nordic Seas and Northern North Atlantic to climate change. In *The Nordic Seas: An integrated perspective, Geophysical Monograph Series* (Vol. 158, pp. 189–197). Washington, DC: American Geophysical Union.

Bellerby, R. G. J., Silyakova, A., Nondal, G., Slagstad, D., Czerny, J., de Lange, T., . . . Discussions, B. (2012). Marine carbonate system evolution during the EPOCA Arctic pelagic ecosystem experiment in the context of simulated Arctic Ocean acidification. *Biogeosciences Discuss*, *9*(11), 15541–15565. https://doi.org/10.5194/bgd-9-15541-2012

Biastoch, A., Treude, T., Rüpke, L. H., Riebesell, U., Roth, C., Burwicz, E. B., . . . Wallmann, K. (2011). Rising Arctic Ocean temperatures cause gas hydrate destabilization and ocean acidification. *Geophysical Research Letters*, *38*, L08602. https://doi.org/10.1029/2011GL047222

Bopp, L., Resplandy, L., Orr, J. C., Doney, S. C., Dunne, J. P., M. Gehlen, . . . Vichi, M. (2013). Multiple stressors of ocean ecosystems in the 21st century: Projections with CMIP5 models. *Biogeosciences*, *10*(10), 6225–6245. https://doi.org/10.5194/bg-10-6225-2013

Boyer, T. P., Antonov, J. I., Baranova, O. K., Coleman, C., Garcia, H. E., Grodsky, A., . . . Zweng, M. M. (2013). *World ocean database 2013, NOAA atlas NESDIS 72* (209 pp.). Silver Spring, MD: National Oceanic and Atmospheric Administration. http://doi.org/10.7289/V5NZ85MT

Caldeira, K., & Wickett, M. E. (2003). Anthropogenic carbon and ocean pH. *Nature*, *425*(September), 365.

Chang, B. X., & Devol, A. H. (2009). Seasonal and spatial patterns of sedimentary denitrification rates in the Chukchi sea. *Deep-Sea Research Part II: Topical Studies in Oceanography*, *56*(17), 1339–1350. https://doi.org/10.1016/j.dsr2.2008.10.024

Ciais, P., Sabine, C., Bala, G., Bopp, L., Brovkin, V., Canadell, J., . . . Thornton, P. (2013). Carbon and other biogeochemical cycles. In T. F. Stocker, et al. (Eds.), *Climate change 2013: The physical science basis. Contribution of working group I to the fifth assessment report of the Intergovernmental Panel on Climate Change* (pp. 465–570). Cambridge, UK: Cambridge University Press.

Cooper, L. W., McClelland, J. W., Holmes, R. M., Raymond, P. A., Gibson, J. J., Guay, C. K., & Peterson, B. J. (2008). Flow-weighted values of runoff tracers (δ18O, DOC, Ba, alkalinity) from the six largest Arctic rivers. *Geophysical Research Letters*, *35*, L18606. https://doi.org/10.1029/2008GL035007

Cornwall, C. E., Boyd, P. W., McGraw, C. M., Hepburn, C. D., Pilditch, C. A., Morris, J. N., . . . Hurd, C. L. (2014). Diffusion boundary layers ameliorate the negative effects of ocean acidification on the temperate coralline macroalga Arthrocardia corymbosa. *PLoS One*, *9*(5), e97235. https://doi.org/10.1371/journal.pone.0097235

Dade, W. B., Hogg, A. J., & Boudreau, B. P. (2001). Physics of flow above the sediment-water interface. In B. P. Boudreau & B. B. Jorgensen (Eds.), *The Benthic boundary layer* (pp. 4–43). New York, NY: Oxford University Press.

Dankers, R., & Middelkoop, H. (2007). River discharge and freshwater runoff to the Barents Sea under present and future climate conditions. *Climatic Change*, *87*(1–2), 131–153. https://doi.org/10.1007/s10584-007-9349-x

Dee, D. P., Uppala, S. M., Simmons, A. J., Berrisford, P., Poli, P., Kobayashi, S., . . . Vitart, F. (2011). The ERA-Interim reanalysis: Configuration and performance of the data assimilation system. *Quarterly Journal of the Royal Meteorological Society*, *137*(656), 553–597. https://doi.org/10.1002/qj.828

Denman, K., Christian, J. R., Steiner, N., Pörtner, H.-O., & Nojiri, Y. (2011). Potential impacts of future ocean acidification on marine ecosystems and fisheries: Current knowledge and recommendations for future research. *ICES Journal of Marine Science*, *68*(6), 1019–1029. https://doi.org/10.1093/icesjms/fsr074

Dickson, A. G. (1984). pH scales and proton-transfer reactions in saline media such as sea water. *Geochimica et Cosmochimica Acta*, *48*(11), 2299–2308.

Dickson, A. G. (1990). Standard potential of the reaction: AgCl(s) + 12H2(g) = Ag(s) + HCl(aq), and the standard acidity constant of the ion HSO4− in synthetic sea water from 273.15 to 318.15 K. *Journal of Chemical Thermodynamics*, *22*(2), 113–127.

Dickson, A. G. (1993). The measurement of sea water pH. *Marine Chemistry*, *44*(2–4), 131–142. https://doi.org/10.1016/0304-4203(93)90198-W

Dickson, A. G., Afghan, J. D., & Anderson, G. C. (2003). Reference materials for oceanic CO_2 analysis: A method for the certification of total alkalinity. *Marine Chemistry*, *80*(2–3), 185–197. https://doi.org/10.1016/S0304-4203(02)00133-0

Dickson, A. G., & Goyet, C. (Eds.). (1994). *Handbook of methods for analysis of the various parameters of the carbon dioxide system in sea water; version 2* (ORNL/CDIAC-74). Washington, DC: U.S. Department of Energy.

Dickson, A. G., Sabine, C. L., & Christian, J. R. (Eds.). (2007). *Guide to best practices for ocean CO_2 measurements (PICES Spec. Publ. 3)*. Sidney, Canada: North Pacific Marine Science Organization.

Dittmar, T., & Kattner, G. (2003). The biogeochemistry of the river and shelf ecosystem of the Arctic Ocean: A review. *Marine Chemistry*, *83*, 103–120. https://doi.org/10.1016/S0304-4203(03)00105-1

Doney, S. C., Fabry, V. J., Feely, R. A., & Kleypas, J. A. (2009). Ocean acidification: The other CO_2 problem. *Annual Review of Marine Science*, *1*, 169–192. https://doi.org/10.1146/annurev.marine.010908.163834

Edmond, J. M. (1970). High precision determination of titration alkalinity and total carbon dioxide content of sea water by potentiometric titration. *Deep-Sea Research and Oceanographic Abstracts*, *17*(4), 737–750. https://doi.org/10.1016/0011-7471(70)90038-0

Fabry, V. J., McClintock, J. B., Mathis, J. T., & Grebmeier, J. M. (2009). Ocean acidification at high latitudes: The Bellweather. *Oceanography*, *22*(4), 160–171. https://doi.org/10.5670/oceanog.2009.105

Fabry, V. J., Seibel, B. A., Feely, R. A., & Orr, J. C. (2008). Impacts of ocean acidification on marine fauna and ecosystem processes. *ICES Journal of Marine Science*, *65*, 414–432.

Feely, R. A., Doney, S. C., & Cooley, S. R. (2009). Ocean acidification: Present conditions and future changes in a high-CO_2 world. *Oceanography*, *22*(4), 36–47.

Flint, M. V. (2010). 54th scientific cruise of research vessel "Akademik Mstislav Keldysh" in the Kara Sea. *Oceanology*, *55*(5), 677–682.

Fransson, A., Chierici, M., Anderson, L. G., Bussmann, I., Kattner, G., Jones, E. P., & Swift, J. H. (2001). The importance of shelf processes for the modification of chemical constituents in the waters of the Eurasian Arctic Ocean: Implication for carbon fluxes. *Continental Shelf Research*, *21*, 225–242.

Frolicher, T. L., & Joos, F. (2010). Reversible and irreversible impacts of greenhouse gas emissions in multi-century projections with the NCAR global coupled carbon cycle-climate model. *Climate Dynamics*, *35*, 1439–1459. https://doi.org/10.1007/s00382-009-0727-0

Frommel, A. Y., Maneja, R., Lowe, D., Malzahn, A. M., Geffen, A. J., Folkvord, A., . . . Clemmesen, C. (2012). Severe tissue damage in Atlantic cod larvae under increasing ocean acidification. *Nature Climate Change*, *2*, 42–46. https://doi.org/10.1038/NCLIMATE1324

Hastie, T., Tibshirani, R., & Friedman, J. (2009). *The elements of statistical learning: Data mining, inference, and prediction* (2nd ed.). New York, NY: Springer-Verlag.

Hauri, C., Gruber, N., Vogt, M., Doney, S. C., Feely, R. A., Lachkar, Z., . . . Plattner, G.-K. (2013). Spatiotemporal variability and long-term trends of ocean acidification in the California Current System. *Biogeosciences*, *10*, 193–216. https://doi.org/10.5194/bg-10-193-2013

Hay, L. E., Wilby, R. L., & Leavesley, G. H. (2000). A comparison of delta change and downscaled GCM scenarios for three mountainous basins in the United States. *Journal of the American Water Resources Association*, *36*(2), 387–397.

Heinze, C. (2004). Simulating oceanic $CaCO_3$ export production in the greenhouse. *Geophysical Research Letters*, *31*, L16308. https://doi.org/10.1029/2004GL020613

Henson, S. A., Beaulieu, C., Ilyina, T., John, J. G., Long, M., Séférian, R., . . . Sarmiento, J. L. (2017). Rapid emergence of climate change in environmental drivers of marine ecosystems. *Nature Communications*, *8*, 14682. https://doi.org/10.1038/ncomms14682

Hibler, W. D., III. (1979). A dynamic thermodynamic sea ice model. *Journal of Physical Oceanography*, *9*(4), 815–846. https://doi.org/10.1175/1520-0485(1979)009<0815:ADTSIM>2.0.CO;2

Holt, J., Allen, J. I., Anderson, T. R., Brewin, R., Butenschön, M., Harle, J., . . . Yool, A. (2014). Challenges in integrative approaches to modelling the marine ecosystems of the North Atlantic: Physics to fish and coasts to ocean. *Progress in Oceanography*, *129*(PB), 285–313. https://doi.org/10.1016/j.pocean.2014.04.024

Holt, J., Hyder, P., Ashworth, M., Harle, J., Hewitt, H. T., Liu, H., . . . Wood, R. (2017). Prospects for improving the representation of coastal and shelf seas in global ocean models. *Geoscientific Model Development*, *10*, 499–523. https://doi.org/10.5194/gmd-2016-145

IPCC. (2000). *Special report on emission scenarios*. Cambridge, UK: Cambridge University Press.

Jakobsson, M., Mayer, L., Coakley, B., Dowdeswell, J. A., Forbes, S., Fridman, B., . . . Weatherall, P. (2012). The International Bathymetric Chart of the Arctic Ocean (IBCAO) version 3.0. *Geophysical Research Letters*, *39*, L12609. https://doi.org/10.1029/2012GL052219

Kaltin, S., & Anderson, L. G. (2005). Uptake of atmospheric carbon dioxide in Arctic shelf seas: Evaluation of the relative importance of processes that influence pCO_2 in water transported over the Bering-Chukchi Sea shelf. *Marine Chemistry*, *94*(1–4), 67–79. https://doi.org/10.1016/j.marchem.2004.07.010

Keup-Thiel, E., Gottel, H., & Jacob, D. (2006). Regional climate simulations for the Barents Sea region. *Boreal Environment Research*, *11*(October), 329–339.

Key, R. M., Olsen, A., van Heuven, S., Lauvset, S. K., Velo, A., Lin, X., . . . Suzuki, T. (2015). *Global ocean data analysis project, Version 2* (GLODAPv2) (ORNL/CDIAC-162, ND-P093). Oak Ridge, TN: Carbon Dioxide Information Analysis Center, Oak Ridge National Laboratory, U.S. Department of Energy. https://doi.org/10.3334/CDIAC/OTG.NDP093_GLODAPv2

Key, R. M., Tanhua, T., Olsen, A., Hoppema, M., Jutterström, S., Schirnick, C., . . . Mintrop, L. (2010). The CARINA data synthesis project: introduction and overview. *Earth System Science Data*, *2*, 105–121.

Koroleff, F. (1972). *Determination of reactive silicate, ICES Cooperative Research Report Series A* (Vol. 29, pp. 87–90). Copenhagen, Denmark: International Council for the Exploration of the Sea.

Kroeker, K. J., Kordas, R. L., Crim, R., Hendriks, I. E., Ramajo, L., Singh, G. S., . . . Gattuso, J.-P. (2013). Impacts of ocean acidification on marine organisms: Quantifying sensitivities and interaction with warming. *Global Change Biology*, *19*, 1884–1896. https://doi.org/10.1111/gcb.12179

Le Quéré, C., Andrew, R. M., Canadell, J. G., Sitch, S., Korsbakken, J. I., Peters, G. P., . . . Zaehle, S. (2016). Global carbon budget 2016. *Earth System Science Data*, *8*(2), 605–649. https://doi.org/10.5194/essd-8-605-2016

Levitus, S., Matishov, G., Seidov, D., & Smolyar, I. (2009). Barents Sea multidecadal variability. *Geophysical Research Letters*, *36*, L19604. https://doi.org/10.1029/2009GL039847

Lindstrom, E. J. (2001). Developing the WOCE global data system. In G. Siedler, J. Church, & J. Gould (Eds.), *Ocean circulation and climate—Observing and modelling the global ocean* (pp. 181–190). Waltham, MA: Academic Press.

Lisitzin, A. P., & Vinogradov, E. M. (1994). The international high-latitude expedition to the Kara Sea (the 49th cruise of the R/V "Dmitry Mendeleev"). *Oceanology*, *34*(5), 643–651.

Loose, B., Miller, L. A., Elliott, S., & Papakyriakou, T. (2011). Sea ice biogeochemistry and material transport across the frozen interface. *Oceanography*, *24*(3), 202–218. https://doi.org/10.5670/oceanog.2011.72

Manizza, M., Follows, M. J., Dutkiewicz, S., Menemenlis, D., McClelland, J. W., Hill, C. N., . . . Key, R. M. (2011). A model of the Arctic Ocean carbon cycle. *Journal of Geophysical Research*, *116*, C12020. https://doi.org/10.1029/2011JC006998

Marchesiello, P., Debreu, L., & Couvelard, X. (2009). Spurious diapycnal mixing in terrain-following coordinate models: The problem and a solution. *Ocean Modelling*, *26*(3–4), 156–169. https://doi.org/10.1016/j.ocemod.2008.09.004

Meehl, G. A., Stocker, T. F., Collins, W. D., Friedlingstein, P., Gaye, A. T., Gregory, J. M., . . . Zhao, Z.-C. (2007). 2007: Global climate projections. In S. Solomon, et al. (Eds.), *Climate change 2007: The physical science basis. Contribution of working group I to the fourth assessment report of the Intergovernmental Panel on Climate Change* (pp. 747–846). Cambridge, UK: Cambridge University Press. https://doi.org/10.1080/07341510601092191

Melsom, A., Lien, V. S., & Budgell, W. P. (2009). Using the Regional Ocean Modeling System (ROMS) to improve the ocean circulation from a GCM 20th century simulation. *Ocean Dynamics*, *59*(6), 969–981. https://doi.org/10.1007/s10236-009-0222-5

Millero, F. J. (1995). Thermodynamics of the carbon dioxide system in oceans. *Geochimica et Cosmochimica Acta*, *59*(4), 661–677. https://doi.org/10.1016/0016-7037(94)00354-O

Millero, F. J. (2010). Carbonate constants for estuarine waters. *Marine and Freshwater Research*, *61*, 139–142.

National Geophysical Data Center. (2006). *2-minute gridded global relief data (ETOPO2) v2*. Silver Spring, MD: NOAA. https://doi.org/10.7289/V5J1012Q

Olafsson, J., Olafsdottir, S. R., Benoit-Cattin, A., Danielsen, M., Arnarson, T. S., & Takahashi, T. (2009a). Rate of Iceland Sea acidification from time series measurements. *Biogeosciences Discuss*, *6*(3), 5251–5270. https://doi.org/10.5194/bgd-6-5251-2009

Olafsson, J., Olafsdottir, S. R., Benoit-Cattin, A., & Takahashi, T. (2009b). The Irminger Sea and the Iceland Sea time series measurements of sea water carbon and nutrient chemistry 1983–2006. *Earth System Science Data Discussions*, *2*(1), 477–492. https://doi.org/10.5194/essdd-2-477-2009

Olli, K., Wexels Riser, C., Wassmann, P., Ratkova, T., Arashkevich, E., & Pasternak, A. (2002). Seasonal variation in vertical flux of biogenic matter in the marginal ice zone and the central Barents Sea. *Journal of Marine Systems*, *38*(1–2), 189–204. https://doi.org/10.1016/S0924-7963(02)00177-X

Olsen, A., Key, R. M., van Heuven, S., Lauvset, S. K., Velo, A., Lin, X., . . . Suzuki, T. (2016). The Global Ocean Data Analysis Project version 2 (GLODAPv2)—An internally consistent data product for the world ocean. *Earth System Science Data*, *8*, 297–323. https://doi.org/10.5194/essd-8-297-2016

Orr, J. C., Fabry, V. J., Aumont, O., Bopp, L., Doney, S. C., Feely, R. A., . . . Yool, A. (2005). Anthropogenic ocean acidification over the twenty-first century and its impact on calcifying organisms. *Nature*, *437*(7059), 681–686. https://doi.org/10.1038/nature04095

Oschlies, A., Schulz, K. G., Riebesell, U., & Schmittner, A. (2008). Simulated 21st century's increase in oceanic suboxia by CO_2-enhanced biotic carbon export. *Global Biogeochemical Cycles*, *22*, GB4008. https://doi.org/10.1029/2007GB003147

Pavlova, G. Y., Tishchenko, P. Y., Volkova, T. I., Dickson, A., & Wallmann, K. (2008). Intercalibration of Bruevich ' s method to determine the total alkalinity in seawater. *Oceanology*, *48*(3), 438–443, https://doi.org/10.1134/S0001437008030168

Popova, E. E., Yool, A., Aksenov, Y., Coward, A. C., & Anderson, T. R. (2014). Regional variability of acidification in the Arctic: A sea of contrasts. *Biogeosciences*, *11*(2), 293–308. https://doi.org/10.5194/bg-11-293-2014

Popova, E. E., Yool, A., Coward, A. C., Aksenov, Y. K., Alderson, S. G., de Cuevas, B. A., & Anderson, T. R. (2010). Control of primary production in the Arctic by nutrients and light: Insights from a high resolution ocean general circulation model. *Biogeosciences*, *7*(11), 3569–3591. https://doi.org/10.5194/bg-7-3569-2010

Pörtner, H. O. (2008). Ecosystem effects of ocean acidification in times of ocean warming: A physiologist's view. *Marine Ecology Progress Series*, *373*(December), 203–217. https://doi.org/10.3354/meps07768

Pörtner, H. O., Karl, D. M., Boyd, P. W., Cheung, W. W. L., Lluch-Cota, S. E., Nojiri, Y., . . . Zavialov, P. O. (2014). Ocean systems. In *Climate change 2014: Impacts, adaptation, and vulnerability. Part A: Global and sectoral aspects. Contribution of working group II to the fifth assessment report of the Intergovernmental Panel on Climate Change* (pp. 411–484). Cambridge, UK: Cambridge University Press. https://doi.org/10.2134/jeq2008.0015br

Renaud, P. E., Sejr, M. K., Bluhm, B. A., Sirenko, B., & Ellingsen, I. H. (2015). The future of Arctic benthos: Expansion, invasion, and biodiversity. *Progress in Oceanography*, *139*, 244–257. https://doi.org/10.1016/j.pocean.2015.07.007

Rhein, M., Rintoul, S. R., Aoki, S., Campos, E., Chambers, D., Feely, R.A., . . . Wang, F. (2013). Observations: Ocean. In T. F. Stocker, et al. (Eds.), *Climate change 2013: The physical science basis. Contribution of working group I to the fifth assessment report of the Intergovernmental Panel on Climate Change* (pp. 255–316). Cambridge, UK: Cambridge University Press.

Riebesell, U., Schulz, K. G., Bellerby, R. G., Botros, M., Fritsche, P., Meyerhöfer, M., . . . Zöllner E. (2007). Enhanced biological carbon consumption in a high CO_2 ocean. *Nature*, *450*(7169), 545–548. https://doi.org/10.1038/nature06267

Rysgaard, S., Glud, R. N., Sejr, M. K., Bendtsen, J., & Christensen, P. B. (2007). Inorganic carbon transport during sea ice growth and decay: A carbon pump in polar seas. *Journal of Geophysical Research*, *112*, C03016. https://doi.org/10.1029/2006JC003572

Sandø, A. B., Melsom, A., & Budgell, W. P. (2014). Downscaling IPCC control run and future scenario with focus on the Barents Sea. *Ocean Dynamics*, *64*(7), 927–949. https://doi.org/10.1007/s10236-014-0731-8

Semiletov, I., Pipko, I., Gustafsson, Ö., Anderson, L. G., Sergienko, V., Pugach, S., . . . Shakhova, N. (2016). Acidification of East Siberian Arctic Shelf waters through addition of freshwater and terrestrial carbon. *Nature Geoscience*, *9*(April), 361–365. https://doi.org/10.1038/NEGO2695

Schneider, B., Engel, A., & Schlitzer, R. (2004). Effects of depth- and CO_2-dependent C:N ratios of particulate organic matter (POM) on the marine carbon cycle. *Global Biogeochemical Cycles*, *18*, GB2015. https://doi.org/10.1029/2003GB002184

Skogen, M. D., Olsen, A., Børsheim, K. Y., Sandø, A. B., & Skjelvan, I. (2014). Modelling ocean acidification in the Nordic and Barents Seas in present and future climate. *Journal of Marine Systems*, *131*, 10–20. https://doi.org/10.1016/j.jmarsys.2013.10.005

Slagstad, D., & McClimans, T. A. (2005). Modeling the ecosystem dynamics of the Barents Sea including the marginal ice zone: I. Physical and chemical oceanography. *Journal of Marine Systems*, *58*(1–2), 1–18. https://doi.org/10.1016/j.jmarsys.2005.05.005

Slagstad, D., & Wassmann, P. (1996). Climate change and carbon flux in the Barents Sea: 3D simulations of ice-distribution, primary production and vertical export of particulate organic carbon. *Memorandum of National Institute of Polar Research*, 51, 119–141.

Slagstad, D., Wassmann, P. F. J., & Ellingsen, I. (2015). Physical constrains and productivity in the future Arctic Ocean. *Frontiers in Marine Science*, *2*(October), 1–23. https://doi.org/10.3389/fmars.2015.00085

Steinacher, M., Joos, F., Frolicher, T. L., Plattner, G., & Doney, S. (2009). Imminent ocean acidification in the Arctic projected with the NCAR global coupled carbon cycle-climate model. *Biogeosciences*, *6*, 515–533.

Steiner, N. S., Christian, J. R., Six, K. D., Yamamoto, A., & Yamamoto-Kawai, M. (2014). Future ocean acidification in the Canada Basin and surrounding Arctic Ocean from CMIP5 earth system models. *Journal of Geophysical Research*: *Ocean*, *119*, 332–347. https://doi.org/10.1002/2013JC009069

Steinhoff, T., Friedrich, T., Hartman, S. E., Oschlies, A., Wallace, D. W. R., & Körtzinger, A. (2010). Estimating mixed layer nitrate in the North Atlantic Ocean. *Biogeosciences*, *7*, 795–807. https://doi.org/10.5194/bgd-6-8851-2009

Stiasny, M. H., Mittermayer, F. H., Sswat, M., Voss, R., Jutfelt, F., Chierici, M., . . . Clemmesen, C. (2016). Ocean acidification effects on Atlantic cod larval survival and recruitment to the fished population. *PLoS One*, *11*(8), e0155448. https://doi.org/10.1371/journal.pone.0155448

Stock, C. A., Alexander, M. A., Bond, N. A., Brander, K., Cheung, W. W. L., Curchitser, E. N., . . . Werner, F. E. (2011). On the use of IPCC-class models to assess the impact of climate on Living Marine Resources. *Progress in Oceanography*, *88*(1–4), 1–27. https://doi.org/10.1016/j.pocean.2010.09.001

Tank, S. E., Raymond, P. A., Striegl, R. G., Mcclelland, J. W., Holmes, R. M., Fiske, G. J., & Peterson, B. J. (2012). A land-to-ocean perspective on the magnitude, source and implication of DIC flux from major Arctic rivers to the Arctic Ocean. *Global Biogeochemical Cycles*, *26*, GB4018. https://doi.org/10.1029/2011GB004192

Tebaldi, C., & Knutti, R. (2007). The use of the multi-model ensemble in probabilistic climate projections. *Philosophical Transactions of the Royal Society A*, *365*, 2053–2075. https://doi.org/10.1098/rsta.2007.2076

Tjiputra, J. F., Assmann, K., Bentsen, M., Bethke, I., Otter, O. H., Sturm, C., & Heinze, C. (2010). Model Development Bergen Earth system model (BCM-C): Model description and regional climate-carbon cycle feedbacks assessment. *Geoscientific Model Development*, *3*, 123–141.

Uppström, L. R. (1974). The boron/chlorinity ratio of deep-sea water from the Pacific Ocean. *Deep-Sea Research and Oceanographic Abstracts*, *21*(2), 161–162.

Vancoppenolle, M., Bopp, L., Madec, G., Dunne, J., Ilyina, T., Halloran, P. R., & Steiner, N. (2013). Future Arctic Ocean primary productivity from CMIP5 simulations: Uncertain outcome, but consistent mechanisms. *Global Biogeochemical Cycles*, *27*, 605–619. https://doi.org/10.1002/gbc.20055

van Heuven, S., Pierrot, D., Rae, J. W. B., Lewis, E., & Wallace, D. W. R. (2011). *MATLAB program developed for CO_2 system calculations* (Rep. ORNL/CDIAC-105b). Oak Ridge, TN:Carbon Dioxide Information Analysis Center, Oak Ridge National Laboratory, U.S. Department of Energy. https://doi.org/10.3334/CDIAC/otg.CO2SYS_MATLAB_v1.1

Vörösmarty, C. J., Fekete, B., & Tucker, B. A. (1996). *River discharge database, version 1.0 (RivDIS v1.0): Volumes 0 through 6. A contribution to IHP-V theme 1. Technical Documents in Hydrology Series*. Paris: UNESCO.

Vörösmarty, C. J., Fekete, B., & Tucker, B. A. (1998). *River discharge database, version 1.1 (RivDISv1.0 supplement)*. Paris: UNESCO.

Wallhead, P. J., Garçon, V., Casey, J. R., & Lomas, M. W. (2014). Long-term variability of phytoplankton carbon biomass in the Sargasso Sea. *Global Biogeochemical Cycles*, *28*, 825–841. https://doi.org/10.1002/2013GB004797

Wassmann, P., Slagstad, D., Riser, C. W., & Reigstad, M. (2006). Modelling the ecosystem dynamics of the Barents Sea including the marginal ice zone: II. Carbon flux and interannual variability. *Journal of Marine Systems*, *59*(1–2), 1–24. https://doi.org/10.1016/j.jmarsys.2005.05.006

Wittmann, A. C., & Pörtner, H.-O. (2013). Sensitivities of extant animal taxa to ocean acidification. *Nature Climate Change*, *3*(11), 995–1001. https://doi.org/10.1038/nclimate1982

Wolf-Gladrow, D. A., Zeebe, R. E., Klaas, C., Kortzinger, A., & Dickson, A. G. (2007). Total alkalinity: The explicit conservative expression and its application to biogeochemical processes. *Marine Chemistry*, *106*(1–2, Special Issue), 287–300. https://doi.org/10.1016/j.marchem.2007.01.006

Wood, E. D., Armstrong, F. A. J., & Richards, F. A. (1967). Determination of nitrate in sea water by cadmium-copper reduction to nitrite. *Journal of the Marine Biological Association of the United Kingdom*, *47*, 23–31. https://doi.org/10.1017/S002531540003352X

Woodgate, R. A., Weingartner, T., & Lindsay, R. (2010). The 2007 Bering Strait oceanic heat flux and anomalous Arctic sea-ice retreat. *Geophysical Research Letters*, *37*, L01602. https://doi.org/10.1029/2009GL041621

Yamamoto, A., Kawamiya, M., Ishida, A., Yamanaka, Y., & Watanabe, S. (2012). Impact of rapid sea-ice reduction in the Arctic Ocean on the rate of ocean acidification. *Biogeosciences*, *9*(6), 2365–2375. https://doi.org/10.5194/bg-9-2365-2012

Yool, A., Popova, E. E., & Coward, A. C. (2015). Future change in ocean productivity: Is the Arctic the new Atlantic? *Journal of Geophysical Research: Oceans*, *120*, 7771–7790. https://doi.org/10.1002/2015JC011167